Cell Reports
Physical Science

CellPress
OPEN ACCESS

Review

1,1-Dicyanomethylene-3-Indanone End-Cap Engineering for Fused-Ring Electron Acceptor-Based High-Performance Organic Photovoltaics

Jiaming Huang,[1,2] Hua Tang,[1] Cenqi Yan,[1,*] and Gang Li[1,2,*]

SUMMARY

Organic photovoltaics (OPVs) have developed rapidly since the advent of fused-ring electron acceptors (FREAs). FREAs bearing bulky fused-ring cores, end-capped with electron-withdrawing groups, present advantages such as broad absorption, tunable frontier orbital levels, and good thermal stability. Recent breakthroughs demonstrate that FREA-based OPVs have achieved more than 17% efficiency, among which the end groups (EGs) of 1,1-dicyanomethylene-3-indanone (IC) and derivatives are critical for the performance enhancement. To date, more than 50 IC derivatives have been reported to construct high-performance FREA-based OPVs. In this review, we first introduce the chemical structure and synthesis route of the IC group. We discuss and classify the recent progress of FREAs based on IC and its derivatives, as well as the impact of IC on the morphology. We consider the issues the IC EGs face, including stability, isomerism, and EG redistribution, finally proposing some future directions for FREAs based on IC and its derivatives.

INTRODUCTION

As a safe, clean, and sustainable energy resource, solar power is an ideal candidate to solve the terawatt challenge with minimal impact of environmental contamination and energy depletion.[1–4] Various photovoltaic technologies, such as crystalline silicon solar cells, copper indium gallium selenide (CIGS) solar cells, and CdTe solar cells, have been developed to convert solar power into electricity. In the past two decades, organic photovoltaics (OPVs) have been a research hotspot by virtue of their low cost, light weight, semi-transparency, and easy fabrication into flexible, large-area devices.[5–9] Currently, power conversion efficiencies (PCEs) of OPVs have been raised to more than 17%, and the development of photoactive materials, in particular fused-ring electron acceptors (FREAs), is the main driving force.

Fullerene acceptors (FAs) have been popular for a long time in OPV fields, since the first report of the bulk heterojunction (BHJ) concept on the basis of a polymer-fullerene system in the 1990s.[10] Many FAs were designed and used in early OPVs, and the most effective ones are $PC_{61}BM$, $PC_{71}BM$, and ICBA. Classic systems such as P3HT/PCBM, PTB7/PCBM, and DTS$(PTTh_2)_2$/PCBM have been systematically researched. Nevertheless, some drawbacks of fullerenes limit the further improvement of FAs. First, FAs have weak absorption in the range of visible and near-infrared (NIR) regions, as the molecular symmetry impedes exciton generation in acceptors. Second, FAs have limited reaction sites, restricting the tunability of structures and

[1]Department of Electronic and Information Engineering, Research Institute for Smart Energy (RISE), The Hong Kong Polytechnic University, Hung Hom, Kowloon, Hong Kong, China

[2]The Hong Kong Polytechnic University Shenzhen Research Institute, Shenzhen 518057, China

*Correspondence:
cenqi.cq.yan@polyu.edu.hk (C.Y.),
gang.w.li@polyu.edu.hk (G.L.)

https://doi.org/10.1016/j.xcrp.2020.100292

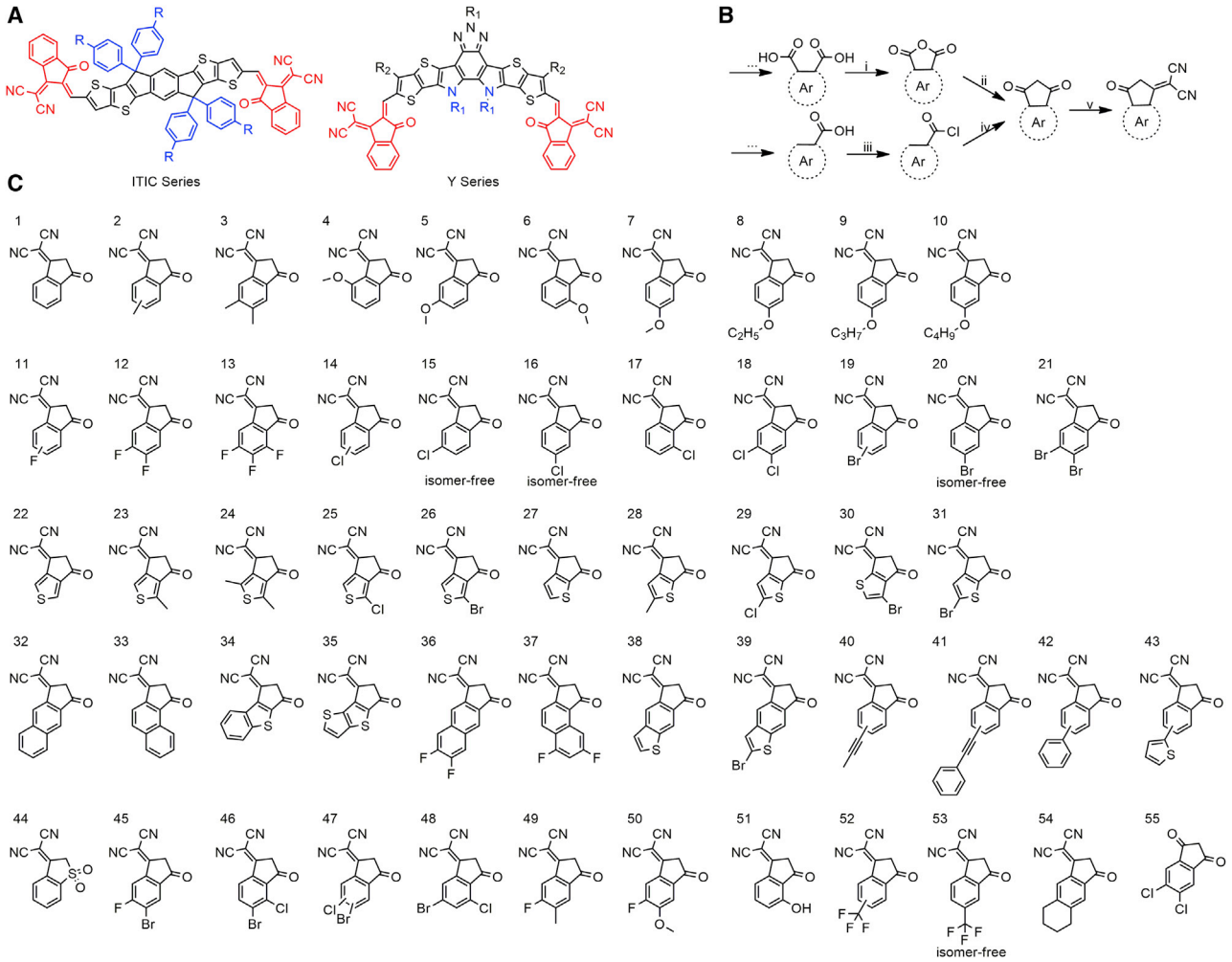

Figure 1. Two Representative FREAs and Their IC EGs, Synthesis Routes, and Derivatives

(A) Chemical structures of ITIC-series and Y-series FREAs.

(B) Synthesis routes of IC. (i) Ac_2O, reflux. (ii) Tert-butyl acetoacetate, Ac_2O/Et_3N, room temperature (RT). (iii) Thionyl chloride, reflux. (iv) Malonyl dichloride, $AlCl_3$, reflux, acidified by HCl. (v) Malononitrile, sodium acetate, RT, acidified by HCl.

(C) Summary of IC and its derivatives.

properties. Third, FAs have poor thermal stability and photochemical stability. Finally, fullerene systems typically exhibit a large energy loss of 0.7–0.9 eV, limiting the open-circuit voltage (V_{OC}).[11,12] Many attempts have been conducted to explore non-fullerene acceptors (NFAs).

As an important class of NFA, FREAs provide the possibility of overcoming the deficiencies of FAs. FREAs, first proposed by Zhan in 2015, have a structure of an A-D-A backbone, consisting of a ladder-type fused-ring core, side chains, end-capped with two electron-deficient chromophoric groups, sometimes with a π-bridge (Figure 1A). Such structures enable FREAs to be used in a modular design, like Lego blocks. These moieties can be easily modified and substituted, which endow FREAs with flexibly tunable structures and properties to match different donor materials. The core, with a sizable conjugated plane, promotes molecule packing and facilitates charge transport. The side chains can adjust the steric hindrance to ensure solution processing and reasonable π-π stacking.

End groups (EGs) of FREAs have a strong electron-withdrawing ability and tunable planarity, which exert significant influence on the optoelectronic properties of FREAs. On the one hand, the strong push-pull effect between the fused-ring core and 1,1-dicyanomethylene-3-indanone (IC) would reduce the optical bandgap and red-shift absorption spectra by downshifting the lowest unoccupied molecular orbital (LUMO) and upshifting the highest occupied molecular orbital (HOMO). The LUMO level can directly affect the V_{OC} of the device. On the other hand, the conjugated plane of EGs facilitates intermolecular π-π stacking and charge transport.

To date, several types of building blocks have been used as EGs for FREAs, such as rhodamine, dicyano rhodamine, cyanide (CN), IC, diketopyrrolopyrrole (DPP), malononitrile, and other chromophoric groups.[13–15] Among these EGs, the most popular and successful groups are the IC group and its derivatives. The benzene ring in the IC group has four positions for modification, and other aromatic rings can substitute the benzene ring. To date, more than 50 IC derivatives have been designed since the introduction of the IC group into FREAs.

In this review, we first introduce the IC group's basics, along with its chemical structure and general synthesis route. Then we discuss recent progress in FREAs based on IC or its derivatives in OPV research, as well as the impact of the IC group on the morphology. Finally, we summarize the key scientific issues to achieve higher efficiency and longer device lifetime, including stability, isomerism, and end-group redistribution. We also propose the future direction of FREAs based on IC and its derivatives, including suppressing the non-radiative recombination loss, improving material stability, simplifying molecules, and reducing cost.

CHEMICAL STRUCTURE OF IC AND ITS DERIVATIVES

The IC group has been widely used in nonlinear optics, organic light-emitting displays, and OPVs.[16,17] Before the invention of the benchmark NFA ITIC, the IC group had been used in polymer donors such as PThTPA-IDT-DCNIO in OPVs.[18] The precursor of the IC group is 1,3-indanedione, featuring a well-conjugated plane. Two carbonyls in first and third positions endow 1,3-indanedione with the electron-deficient property. The IC group is obtained by introducing malononitrile into the first position, which further strengthens the electron-withdrawing ability.[19] The substitution of one malononitrile would not introduce the massive steric hindrance and would not influence indanedione's planarity because of the linear -C≡N group with sp hybridization[20]. Further introducing malononitrile in the third position of 1,3-indanedione would render the molecule unstable because of the high strain between the core and EG unit.[19,21]

Typically, IC can be obtained by two typical synthetic routes (Figure 1B). One starts with the aromatic ring -*o*-dicarboxylic acid converted to the anhydride via intramolecular dehydration (reaction i). The diketone is obtained through the condensation of anhydride (reaction ii). Another route begins with an aromatic ring carboxylic acid, which is chlorinated by the thionyl chloride to obtain the acyl chloride (reaction iii). The diketone is obtained by Friedel-Crafts acylation (reaction iv). Malononitrile is incorporated in one carbonyl to obtain the final EGs (reaction v).

The modification method of the classic IC group can be classified into the following categories: (1) IC group with alkyl/halogen substitution, (2) thienyl-fused IC group (TC), (3) π-extended IC group, (4) other IC-based EG, and (5) asymmetric substitution. The reported IC-based derivatives are summarized in Figure 1C.

RECENT PROGRESS IN FREAs ACCORDING TO IC EGs

IC Group: The Basics

The first landmark FREA, ITIC, was reported in 2015.[22] ITIC has a fused heptacyclic core, IDTT, connected with the IC group and four alkylbenzene side chains. ITIC shows a PCE of 6.8% when blended with the PTB-series polymeric donor PTB7-Th.[23] This work first demonstrates that NFAs have comparable or even better performance relative to FAs. The efficiency was further improved to 11% when paired with polymeric donor PBDB-T.[24] After these successes, FREAs have experienced rapid development in the past 4 years. All the parameters of devices mentioned in this review are summarized in Table 1.

Various fused-ring cores are paired with the IC EGs to construct FREAs. For the fused heptacyclic FREAs, ITIC-Th was obtained by replacing alkylbenzene in ITIC with thienyl side chains (Figure 2).[25] ITIC-Th with thienyl side chains has a lower frontier orbital (−5.66/ −3.93 eV) than ITIC (−5.48/ −3.83 eV) because of the σ-inductive effect of thienyl. Meanwhile, sulfur-sulfur interaction between two adjacent thienyl groups leads to stronger π-π stacking and higher electron mobility.[26,27] Consequently, ITIC-Th devices show an optimal PCE of 9.6% and better photo-stability than ITIC.[28] An n-hexyl was introduced into the β-position of the fringe thienyl of ITIC to afford ITC6-IC.[29] Comparing ITIC and ITIC-Th, the introduction of hexyl onto the central core benefits the formation of a definite configuration with a planar structure and weaker π-π stacking. The weak electron-pushing n-hexyl also slightly upshifts the LUMO level of ITC6-IC and improves V_{OC}. Finally, devices based on PBDB-T: ITC6-IC achieve a high PCE of 11.6% with an expected high V_{OC} of 0.97 V. This strategy of locking conformation has been adopted in the later work of A-DA¢D-A backbone FREAs and shows great importance, which will be discussed later.

Another type of fused heptacyclic acceptor uses a benzo[1,2-b:4,5-b]dithiophene (BDT) center core. For instance, NFBDT (ITIC1), an isomer of ITIC, was designed featuring a benzodi(cyclopentadithiophene) core.[30,31] Devices based on PBDB-T: NFBDT show an efficiency of 10.42%. In NFBDT (ITIC1), the position of C (sp^3) is farther from the central benzene ring relative to ITIC, which makes the modification of H in the benzene ring possible because of the smaller steric hindrance. In this case, NFBDT derivatives with alkoxy and thienyl substituted in the central benzene were obtained, called BT-IC and ITIC2.[32] The alkoxyl side chain with electron-donating ability upshifts the HOMO to −5.32 eV, while the electron-withdrawing thienyls downshift the HOMO to −5.43 eV, compared with NFBDT with a HOMO of −5.40 eV. Compared with alkoxyl, the thienyl side chain can extend the conjugated plane, which benefits absorption and facilitates π-π stacking. Along with the polymeric donor FTAZ, ITIC2 exhibits a higher PCE of 11% with a higher J_{SC} of 18.88 mA/cm^2 and FF of 0.63 compared with NFBDT (ITIC1).

FREAs based on other fused-ring cores have also been reported. For example, IDIC and IC-1IDT-IC (IDTIC) were synthesized on the basis of a pentacyclic IDT unit. Through tuning sidechains, the photovoltaic performance on the basis of IDTIC and IDIC is 7.39% and 9.20%. Because of the short conjugation length, fused pentacyclic electron acceptors typically exhibit inferior performance to heptacyclic FREAs. To further modify pentacyclic FREAs, a π-bridge can be introduced between the fused-ring core and EGs.[33] For example, a NIR FREA, SJ-IC, can be obtained by introducing a double-bond π-bridge into IDTIC. Double bonds effectively red-shift absorption, improve electron mobility, and tune crystallinity, which endows J61: SJ-IC blend with appropriate phase separation. SJ-IC demonstrates a high PCE of 9.27% with improved

Table 1. Parameters of Devices Based on FREAs Discussed in This Review

Name	E_g (eV)	HOMO (eV)	LUMO (eV)	Donor	V_{OC} (V)	J_{SC} (mA/cm^2)	FF	PCE (%)	Reference
ITIC	1.59	−5.48	−3.83	PBDB-T	0.90	16.8	0.74	11.21	22
ITIC-Th	1.60	−5.66	−3.93	PDBT-T1	0.88	16.24	0.67	9.60	25
ITC6-IC	1.60	−5.73	−3.92	PBDB-T	0.97	16.41	0.73	11.61	29
NFBDT	1.56	−5.40	−3.83	PBDB-T	0.87	17.85	0.67	10.42	30
ITIC1	1.55	−5.48	−3.84	FTAZ	0.92	15.67	0.56	8.09	31
BT-IC	1.43	−5.32	−3.85	J71	0.90	17.75	0.66	10.28	32
ITIC2	1.53	−5.43	−3.80	FTAZ	0.93	18.88	0.63	11.00	31
IDIC	1.62	−5.69	−3.91	PTFBDT-BZS	0.91	17.30	0.71	11.03	54
IC-1IDT-IC	1.72	−5.69	−3.88	J61	0.88	13.70	0.57	6.95	55
SJ-IC	1.49	−5.61	−3.94	J61	0.83	16.99	0.66	9.27	34
IEIC	1.57	−5.42	−3.82	PTB7-Th	0.97	13.55	0.48	6.31	35
IEICO	1.34	−5.32	−3.95	PBDTTT-E-T	0.82	17.70	0.58	8.40	36
IDT-BC6	1.75	−5.55	−3.82	PBDB-T	0.92	5.63	0.44	2.30	37
IDT-BOC6	1.63	−5.51	−3.78	PBDB-T	1.01	15.35	0.54	8.49	37
IHIC-N	1.66	−5.58	−3.81	PTB7-Th	0.85	13.50	0.61	6.91	38
IHIC	1.38	−5.45	−3.93	PTB7-Th	0.75	19.01	0.68	9.77	39
IT-M	1.60	−5.58	−3.98	PBDB-T	0.94	17.44	0.74	12.05	49
IT-DM	1.63	−5.56	−3.93	PBDB-T	0.97	16.48	0.71	11.29	49
IT-OM-1	1.67	−5.50	−3.76	PBDB-T	1.01	12.31	0.51	6.30	56
IT-MO-3	1.64	−5.52	−3.80	PBDB-T	0.97	14.69	0.56	7.90	56
IT-OM-4	1.63	−5.49	−3.81	PBDB-T	0.96	16.38	0.68	10.80	56
IT-O2	1.59	−5.49	−4.01	PBDB-T	0.97	15.34	0.63	9.30	57
IT-O3	1.59	−5.48	−3.97	PBDB-T	0.98	9.80	0.51	4.90	57
IT-O4	1.59	−5.47	−3.99	PBDB-T	0.95	9.16	0.48	4.20	57
IT-2F	1.55	−5.54	−3.9	PBDB-T	0.83	18.62	0.71	10.98	58
IT-4F	1.55	−5.66	−4.14	PBDB-T-2F	0.87	20.38	0.77	13.70	59
ITIC-6F	1.51	−5.78	−4.16	PBDB-T-2F	0.82	21.60	0.67	11.41	60
INIC	1.57	−5.45	−3.88	FTAZ	0.96	13.50	0.58	7.70	61
INIC1	1.56	−5.54	−3.97	FTAZ	0.93	16.60	0.64	10.10	61
INIC2	1.52	−5.52	−3.98	FTAZ	0.90	17.60	0.67	10.80	61
INIC3	1.48	−5.52	−4.02	FTAZ	0.85	19.68	0.69	11.50	61
ITIC-Th1	1.55	−5.74	−4.01	FTAZ	0.85	19.33	0.74	12.10	62
ITIC-Th2	1.54	−5.43	−3.80	FTAZ	0.92	18.63	0.62	10.60	62
POIT-IC	1.58	−5.57	−3.92	PBDB-T-2F	1.04	16.10	0.60	10.10	63
POIT-IC2F	1.55	−5.62	−4.01	PBDB-T-2F	0.97	18.60	0.69	12.40	63
POIT-IC4F	1.49	−5.65	−4.07	PBDB-T-2F	0.91	20.90	0.73	13.80	63
m-ITIC	1.58	−5.52	−3.82	J61	0.91	18.31	0.71	11.77	64
m-ITIC-2F	1.56	−5.73	−3.95	PTQ10	0.96	18.98	0.69	12.53	64
m-ITIC-4F	1.53	−5.73	−4.02	PTQ10	0.90	19.76	0.70	12.53	64
IT-2Cl	1.48	−5.75	−4.09	PBDB-T	0.74	21.50	0.60	9.10	65
IT-4Cl	1.52	−5.68	−3.99	PBDB-T-2F	0.90	18.03	0.67	10.85	65
BDSeIC	1.51	−5.53	−3.92	PBDB-T-2F	0.97	14.00	0.52	7.10	66
BDSeIC2Br	1.41	−5.63	−3.99	PBDB-T-2F	0.89	20.30	0.69	12.50	66
BDSeIC4Br	1.39	−5.65	−4.02	PBDB-T-2F	0.85	16.40	0.69	9.60	66
BT-ClC	1.33	−5.49	−4.09	PTB7-Th	0.70	22.50	0.71	11.20	67
IEICO-4Cl	1.23	−5.56	−4.23	PTB7-Th	0.73	22.80	0.62	10.30	68
IEICO-4F	1.24	−5.44	−4.19	PTB7-Th	0.73	25.30	0.59	10.90	69
ITCC	1.67	−5.47	−3.76	PBDB-T	1.01	15.90	0.71	11.40	70
ITTC	1.58	−5.62	−3.96	PBDB-T-2F	0.97	17.13	0.74	12.31	71
ITCPTC	1.58	−5.62	−3.96	PBT1-EH	0.95	16.50	0.75	11.80	72
ITCC-M	1.68	−5.50	−3.67	PBDB-T	1.03	14.80	0.66	10.10	73
MeIC	1.58	−5.57	−3.92	PBDB-T-2F	0.99	18.47	0.71	13.04	74
ITCT-DM	1.58	−5.48	−3.90	PBDB-T	0.90	17.42	0.65	10.56	75
C8-ITCC	1.66	−5.45	−3.85	PBDB-T-2F	1.04	16.10	0.63	10.50	76

(*Continued on next page*)

Table 1. *Continued*

Name	E_g (eV)	HOMO (eV)	LUMO (eV)	Donor	V_{OC} (V)	J_{SC} (mA/cm^2)	FF	PCE (%)	Reference
C8-ITCC-Cl	1.58	−5.50	−3.93	PBDB-T-2F	0.96	18.00	0.74	12.70	76
4TTIC	1.46	−5.46	−3.73	PBDB-ST	0.93	18.56	0.67	11.48	77
4TTIC-Cl	1.42	−5.50	−3.79	PBDB-ST	0.88	20.19	0.74	13.11	77
ITC-2Cl	1.58	−5.58	−4.01	PBDB-T-2Cl	0.92	20.17	0.74	13.66	78
ITC-2Br	1.73	−5.73	−3.93	PBDB-T-2F	1.03	15.40	0.69	11.90	79
ITC-2Br1	1.70	−5.70	−3.95	PBDB-T-2F	1.01	16.60	0.71	10.90	79
ITC-2Br2	1.59	−5.59	−4.02	PBDB-T-2F	0.90	19.80	0.74	13.10	79
IDTN	1.59	−5.79	−3.98	PBDB-T-2F	0.95	16.58	0.78	12.20	80
ITN-C9	1.54	−5.78	−3.92	PBDB-T-2F	0.92	15.68	0.65	9.33	81
ITzN-C9	1.56	−5.62	−3.78	PBDB-T-2F	1.05	14.12	0.64	9.51	81
ITBTC	1.61	−5.38	−3.78	PBDB-T	0.94	16.37	0.71	10.99	82
ITBC	1.59	−5.49	−3.90	PBDB-T	0.94	19.90	0.65	12.07	83
BDCPDT-TTC	1.58	−5.38	−3.78	PBDB-T	0.94	17.72	0.62	10.29	84
ITN-F4	1.49	−6.1	−4.3	PBDB-T-2F	0.82	19.60	0.67	10.70	85
ITzN-F4	1.58	−6.0	−4.2	PBDB-T-2F	0.92	17.50	0.68	10.90	85
BDSe2(BrCl)	1.39	−5.64	−3.95	PBDB-T-2Cl	0.83	22.91	0.77	14.54	86
ITCF	1.57	−5.59	−3.95	J71	0.91	18.48	0.79	13.25	87
IDT-IC-T	1.67	−5.72	−3.91	PBDB-T	0.85	15.73	0.70	9.43	88
IDT-IC-B	1.66	−5.75	−3.92	PBDB-T	0.87	14.13	0.70	8.72	88
FO-PCIC	1.59	−5.49	−3.75	PBDB-T	0.90	15.02	0.61	8.29	89
ITPN	1.60	−5.69	−3.91	PBDB-T-2F	0.99	17.50	0.73	12.60	90
ITEN	1.58	−5.63	−3.90	PBDB-T-2F	0.99	16.50	0.67	10.90	90
IDT-HN	1.68	−5.92	−3.86	PBDB-T	0.93	14.43	0.76	10.22	91
IT-OH	1.54	−5.57	−3.92	PBDB-T	0.89	16.71	0.70	10.40	92
IT-DOH	1.53	−5.58	−3.93	PBDB-T-2F	0.96	17.78	0.73	12.50	92
ITCF3	1.49	−5.71	−3.97	PBDB-T-2F	0.84	20.90	0.76	13.30	93
ITTBC	1.53	−5.61	−4.13	PBDB-T-2F	0.86	12.52	0.63	6.83	94
ITThBC	1.58	−5.71	−4.15	PBDB-T-2F	0.87	13.36	0.65	7.59	94
IO-4Cl	1.80	−5.72	−3.83	PBDB-T-2F	1.24	11.60	0.68	9.80	95
α-IT-2F	1.56	−5.67	−4.07	PBDB-T	0.78	19.06	0.69	10.28	96
α-IT-2OM	1.63	−5.61	−3.92	PBDB-T	0.93	18.11	0.72	12.07	96
α-ITIC-2Cl	N/A	−5.29	−3.77	PBDB-T-2F	0.88	18.91	0.74	12.23	97
ITIC-2Cl-β	N/A	−5.30	−3.71	PBDB-T-2F	0.94	18.47	0.65	11.21	97
IDTT-2F-Th	1.55	−5.78	−4.09	PBT1-C-2Cl	0.91	17.82	0.74	12.01	98
ITIC-Cl⁻δ-Th	N/A	−5.31	−3.70	PBDB-T-2F	0.86	18.58	0.72	11.45	99
ITIC-Cl⁻γ-Th	N/A	−5.30	−3.66	PBDB-T-2F	0.91	18.30	0.73	12.25	99
ITIC-2Cl-Th	N/A	−5.31	−3.74	PBDB-T-2F	0.89	17.27	0.73	11.13	99
ITIC-2Cl-δ	N/A	−5.53	−3.94	PBDB-T-2F	0.90	18.34	0.70	11.51	100
ITIC-2Cl-γ	N/A	−5.55	−3.92	PBDB-T-2F	0.93	18.94	0.74	13.03	100
ITIC-2Br-m	1.52	−5.53	−3.90	PBDB-T-2F	0.87	18.01	0.70	10.88	101
ITIC-2Br-γ	1.53	−5.54	−3.90	PBDB-T-2F	0.89	19.01	0.71	12.05	101
COi6-2Cl-m	1.31	−5.47	−4.02	PTB7-Th	0.69	20.78	0.64	9.22	102
COi6-2Cl-δ	1.31	−5.46	−4.02	PTB7-Th	0.67	20.65	0.61	8.41	102
COi6-2Cl-γ	1.31	−5.46	−4.05	PTB7-Th	0.69	20.33	0.63	8.82	102
ITIC-γCl⁻2F	N/A	−5.52	−3.88	PBDB-T-2F	0.85	19.60	0.73	12.02	103
Y1	1.44	−5.45	−3.95	PBDB-T	0.87	22.44	0.69	13.42	40
Y5	1.38	−5.55	−3.87	PBDB-T	0.87	22.60	0.71	14.00	44
BTP-M	1.42	−5.47	−3.81	PBDB-T	0.90	23.06	0.69	14.24	104
Y8	1.41	−5.54	−3.84	PBDB-T	0.76	25.74	0.71	14.06	42
Y6	1.33	−5.65	−4.10	PBDB-T-2F	0.83	25.30	0.75	15.70	105
Y1-4F	1.31	−5.56	−4.11	PBDB-T-2F	0.83	25.20	0.69	14.80	106
Y9	1.36	−5.59	−3.78	PBDB-T	0.90	23.28	0.63	13.26	107
Y14	1.30	−5.56	−4.01	PBDB-T	0.80	26.15	0.71	14.92	108
BTP-0F	N/A	−5.59	−3.79	PBDB-T-2F	0.96	15.20	0.57	8.20	109

(*Continued on next page*)

Table 1. *Continued*

Name	E_g (eV)	HOMO (eV)	LUMO (eV)	Donor	V_{OC} (V)	J_{SC} (mA/cm^2)	FF	PCE (%)	Reference
BTP-2F	N/A	−5.64	−3.85	PBDB-T-2F	0.89	22.10	0.72	14.10	[109]
BTP-4F	N/A	−5.68	−3.89	PBDB-T-2F	0.85	25.30	0.78	16.70	[109]
BTP-6F	N/A	−5.69	−3.97	PBDB-T-2F	0.81	25.90	0.73	15.30	[109]
Y15	1.30	−5.56	−3.92	PBDB-T-2F	0.88	23.79	0.68	14.13	[110]
BTP-4Cl	1.33	−5.68	−4.12	PBDB-T-2F	0.87	25.40	0.75	16.50	[111]
BTP-4Cl-12	N/A	−5.66	−4.09	PBDB-T-2F	0.86	25.60	0.78	17.00	[112]
N3-4Cl	1.35	−5.63	−3.98	PBDB-T-2F	0.85	25.90	0.75	16.53	[113]
BTP-4F-12	1.33	−5.68	−4.06	PBDB-T-2F	0.86	25.30	0.76	16.40	[114]
N3	N/A	−5.65	−4.09	PBDB-T-2F	0.84	25.81	0.74	15.98	[115]
Y2	1.32	−5.43	−4.04	PBDB-T	0.82	23.56	0.69	13.40	[40]
Y6-T	1.35	−5.51	−3.90	PBDT-ST	0.92	22.56	0.70	14.35	[116]
BTCT-2Cl	1.37	−5.56	−3.95	PBDB-T-2F	0.88	24.40	0.70	15.10	[117]
BTTPC	1.39	−5.47	−3.78	PBDB-T	0.89	22.25	0.73	14.51	[118]
BTTPC-Br	1.37	−5.38	−3.45	PBDB-T	0.86	24.71	0.71	15.22	[118]
BTP-ClBr	1.38	−5.79	−4.00	PBDB-T-2F	0.91	23.48	0.79	16.82	[119]
BTIC-CF3-m	1.31	−5.45	−3.97	PBDB-T-2F	0.85	24.89	0.72	15.30	[120]
BTIC-CF3-γ	1.30	−5.45	−3.96	PBDB-T-2F	0.86	25.19	0.73	16.59	[120]
BTIC-γCl$^-$2F	1.35	−5.39	−3.87	PBDB-T-2F	0.86	24.60	0.73	15.43	[103]
ZY-4Cl	N/A	−5.64	−3.67	P3HT	0.88	16.49	0.65	9.46	[121]
BTP-IS	1.42	−5.65	−4.02	PBDB-T-2F	0.89	22.63	0.63	12.79	[122]
BTP-S1	1.49	−5.55	−4.01	PBDB-T-2F	0.93	22.39	0.73	15.21	[123]
BTP-S2	1.48	−5.65	−4.01	PBDB-T-2F	0.95	24.07	0.72	16.37	[123]
SY1	N/A	−5.68	−3.95	PBDB-T-2F	0.87	25.41	0.76	16.83	[124]
SY2	N/A	−5.67	−3.99	PBDB-T-2F	0.85	25.29	0.74	16.01	[124]
SY3	N/A	−5.69	−3.98	PBDB-T-2F	0.86	25.54	0.74	16.23	[124]
BTP-2F-ThCl	1.34	−5.70	−3.99	PBDB-T-2F	0.87	25.38	0.77	17.06	[125]
BTIC-2Cl-γCF3	N/A	−5.55	−4.00	PBDB-T-2F	0.84	25.09	0.77	16.31	[126]

J_{SC} and FF compared with IDTIC.[34] Additionally, aromatic groups such as phenyl and thienyl are used as π-bridges to extend the conjugated length of IDTIC and afford NFAs including IEIC, IEICO, IDT-BC6, and IDT-BOC6.[35–37] Fused hexacyclic electron acceptors (IHIC-N and IHIC) are delivered by replacing the central benzene in the IDT unit with naphthalene and thieno[3,2-b]thiophene (TT), respectively.[38,39] Compared with naphthalene and benzene, TT with electron-donating ability increases the intramolecular charge transfer (ICT) effect and thus extends the absorption to the NIR region. The HOMO/LUMO levels of IHIC-N and IHIC are −5.58/−3.81 eV and −5.45/−3.93 eV, respectively. The optical bandgap (E_g^{opt}) of IHIC (1.38 eV) is much smaller than IHIC-N (1.66 eV). As a result, devices based on PTB7: IHIC show a PCE of 10.6% with a high J_{SC} over 19 mA/cm^2 in comparison with PTB7: IHIC-N (PCE of 6.91% and J_{SC} of 13.5 mA/cm^2).

A new type of FREA with the A-DA¢D-A structure core and IC units has achieved the highest PCE in the field of OPVs.[40] Taking Y1 as an example, it is built with an electron-deficient central core of benzotriazoles. Nitrogen-heteroatomic bridges and thiophene units further extend the conjugation. Alkyl side chains are connected in nitrogen atoms of the core to prevent excessive aggregation. The sp^2 hybridized nitrogen not only provides stronger electron-donating ability but also maintains smaller steric hindrance to the sp^3 hybridized carbon, which connects side chains. It facilitates π-π stacking and benefits charge transport.[41] Moreover, the twisted electron-deficient core results in the formation of two planar units in the acceptor. This twisted structure between D-A units may lead to enhanced spin-orbital coupling, as well as a decreased gap between singlet (S) and triplet (T). This small

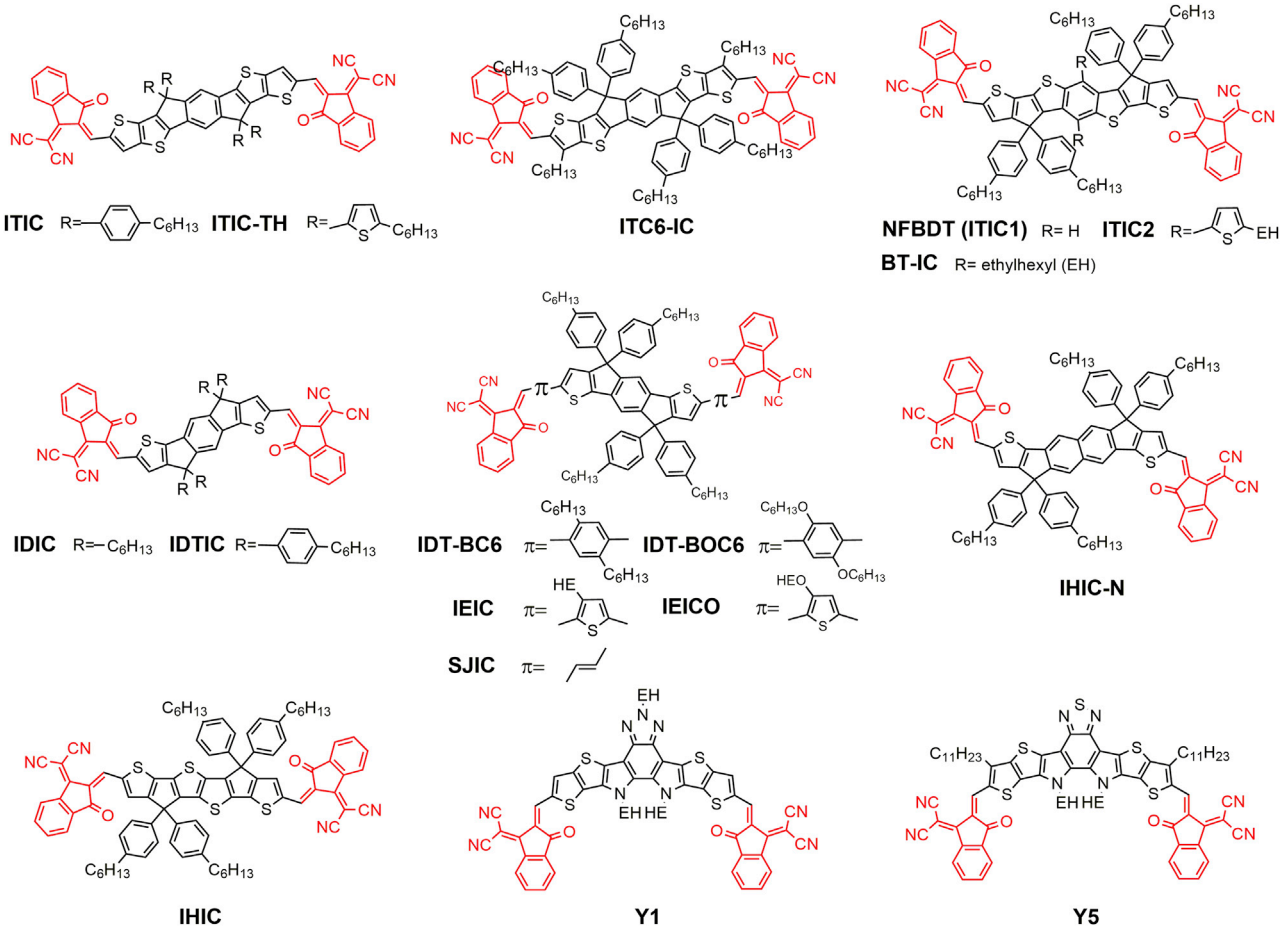

Figure 2. Chemical Structures of FREAs Based on IC

offset ΔE_{ST} can facilitate intersystem crossing (ISC), thus generating triplet excitons and contributing to J_{SC}.[42] Last, this A-DA¢D-A FREA with a unique banana shape that differs from ITIC can enlarge the conjugation to form a polymer-like backbone and then achieve a three-dimensional (3D) interpenetrating network.[43] As a result, Y1 featuring the A-DA¢D-A structure exhibits a HOMO of −5.45 eV and a LUMO of −3.95 eV and shows strong absorption in the NIR range. Compared with PBDB-T: ITIC, PBDB-T: Y1 shows a higher PCE of 13.4% with a low voltage loss (V_{loss}) and a high J_{SC} of 22.0 mA/cm^2. Y5 is obtained by replacing the central core benzotriazole in Y1 with benzothiadiazole (BT).[44] Three medium bandgap polymers (PBDB-T, TTFQx-T1, and J61) have been paired with Y5, obtaining PCEs of 14.1%, 13.1%, and 11.0%, respectively. All these devices show high J_{SC} values of more than 21 mA/cm^2, because of complementary absorption.

FREAs based on IC EGs have already achieved very encouraging PCEs of 15%, which demonstrates the potential of IC end groups and arouses researchers' attention. The IC EG has many transformation ways. It has four grafting sites, and the benzene ring in IC can be replaced or expanded. Therefore, researchers have begun to explore the structure-property relationship of IC derivative and FREAs, using alkyl and alkoxyl substitution, halogen substitution, TC, π-extension, and asymmetric substitution to further fine-tune frontier orbital levels, absorption, molecular conformation

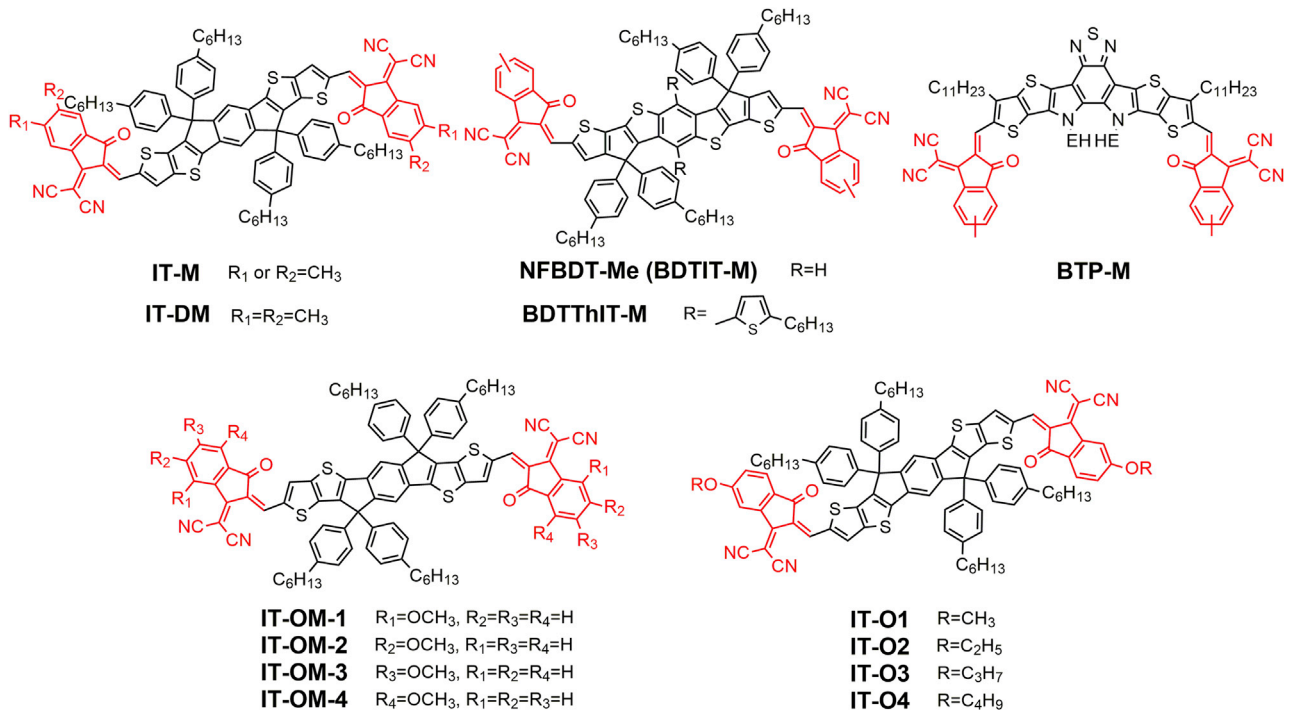

Figure 3. Chemical Structures of FREAs Based on Alkylated/Alkoxylated IC

and packing, electron mobility, and the final device performance of FREAs, which will be carefully discussed in the following.

IC Group with Alkyl and Alkoxyl Substitution

Alkyl and alkoxyl have been used to modify the IC end group (Figure 3).[45–48] In principle, the introduction of a weak electron-donating unit would reduce the electron-withdrawing ability of EGs, weaken the ICT effect, and elevate the LUMO of the whole acceptor, thus increasing the V_{OC} of the device. IT-M and IT-DM were reported by introducing methyl into the IC end group of ITIC.[49] This weak electron-donating methyl weakens ICT effect, blue-shifts the absorption, and upshifts the LUMO levels. Consequently, high V_{OC} values of 0.94 and 0.97 V, together with PCEs of 12.05% and 11.29%, are obtained from the devices based on PBDB-T: IT-M and PBDB-T: IT-DM, compared with PBDB-T: ITIC (V_{OC} = 0.90 V, PCE = 11.22%). Ye et al.[50] presented a quantitative study of the multi-length scale morphology of high-performance FREA-based OPVs. They found direct correlations between device characteristics and morphological attributes at small length scales for OPVs based on PBDB-T: IT-M and PBDB-T: IT-DM. A strong correlation was observed between the average purity at a 10 nm length scale, FF, and J_{SC}. More important, the investigators found that the temperature-dependent Flory-Huggins interaction parameter (χ) could be the critical factor in controlling the average purity at a small length scale. The estimated χ parameter of the PBDB-T: IT-M blend at room temperature is obviously higher (»2.7) than that of the PBDB-T: IT-DM blend (»2.0). Xie et al.[51] found that PBDB-T: IT-M system exhibits smaller energetic disorder than PBDB-T: ITIC, which contributes to the smaller V_{OC} loss of PBDB-T: IT-M. Likewise, NFBDT-Me (BDTIT-M) was obtained by methylating the IC EG of NFBDT, which enhanced the LUMO level by about 0.5 eV.[52,53] BDTIT-M-based OPVs exhibit a higher V_{OC} of 0.903 V and a PCE of 11.31% compared with their NFBDT-based counterparts (V_{OC} = 0.868 V, PCE = 10.42%).

BTP-M was synthesized by methylating the IC termini of Y5.[104] Compared with Y5, BTP-M exhibited an upshifted HOMO of −5.47 eV and a LUMO of −3.81 eV. Along with PM6, BTP-M exhibited a high V_{OC} of 0.975 V but a low PCE of 4.26%. Monomethyl in EGs of BTP-M reduces the intermolecular interactions and prevents over-aggregation of acceptors and tunes the phase separation of blending film. Via the formation of acceptor alloy, the PM6: Y6: BTP-M ternary device shows a PCE of more than 17%, with improved V_{OC} and J_{SC} relative to PM6: Y6.

Alkyoxyl groups have a strong electron-donating conjugative but a weak electron-withdrawing inductive effect. Methoxyl shows stronger electron-pushing ability than methyl and can more effectively elevate the LUMO of the acceptor when introduced into the EGs. Li et al.[56] synthesized four isomers, IT-OM-(1, 2, 3, 4), with different substitution sites of the methoxyl on the IC termini to systematically investigate the substitution position effects in FREAs. All these isomers with strong electron-donating methoxyls exhibit higher LUMO levels than IT-M. The positions of methoxyl influence the frontier orbital levels, molecular configuration, and active layer morphology. The molecular planarity is well maintained when the methoxy group is in the 5- or 6-position (IT-OM-2 and IT-OM-3), while EGs with methoxyl in the 4- and 7-positions (IT-OM-1 and IT-OM-4) exhibit distortions and hinder the intermolecular packing. Compared with its isomeric counterparts, IT-OM-2 exhibits stronger crystallinity, higher electron mobility, and a higher PCE of 11.9% with a J_{SC} value of 17.53 mA/cm^2 and FF of 0.73. These results illustrate that better molecular ordering in the blend driven by favorable methoxylation enhances exciton dissociation balance charge transport, thus improving J_{SC} and FF.

Molecular dynamics simulations and long-range corrected density functional theory calculations are further combined to describe relationships among the chemical structure, local morphology, and electronic properties of PBDB-T/IT-OM-(1,2,4) blends at the molecular scale.[127–129] Brédas and coworkers found the following: (1) The methoxyl location affects the χ value of the blends by varying the intermolecular interactions between PBDB-T and IT-OM. The larger χ for PBDB-T/IT-OM-4 can result in weaker mixing, in line with the obvious phase separation measured experimentally. (2) The energies of the charge transfer (CT) states follow the variations in electron affinities of IT-OM-(1,2,4): IT-OM-1 > IT-OM-4 > IT-OM-2. The smaller electronic couplings and energy differences between the local exciton (LE) and CT states, and larger reorganization energies, result in lower exciton dissociation of PBDB-T/IT-OM-1. As a comparison, the methoxyl position hardly influences radiative and non-radiative recombination rates, resulting in similar $E_{loss}^{non,rad}$ in these blends. (3) The higher electron mobility of PBDB-T/IT-OM-2 is ascribed to the faster intermolecular electron transfer rates between adjacent molecules calculated than that in PBDB-T/IT-OM-1 and the larger acceptor π-π packing density than that in PBDB-T/IT-OM-4. The superior performance of PBDB-T/IT-OM-2-based OPVs can be ascribed to suitable phase separation, higher interfacial exciton dissociation rates, and more efficient electron transport.

Zhu et al.[57] designed a series of dithienoindaceno[1,2-b:5,6-b′] dithiophene (DT-IDT) based FREAs, IT-O(1-4), with increased alkoxyl chain length from methoxyl to butoxyl on the EGs. Solubility and electron mobility are both improved with the decreased length of side chains, leading to ideal morphology and balanced charge transport. Consequently, the PBDB-T: IT-O1 system exhibited higher J_{SC} and FF and an obviously higher PCE of 11.6%.

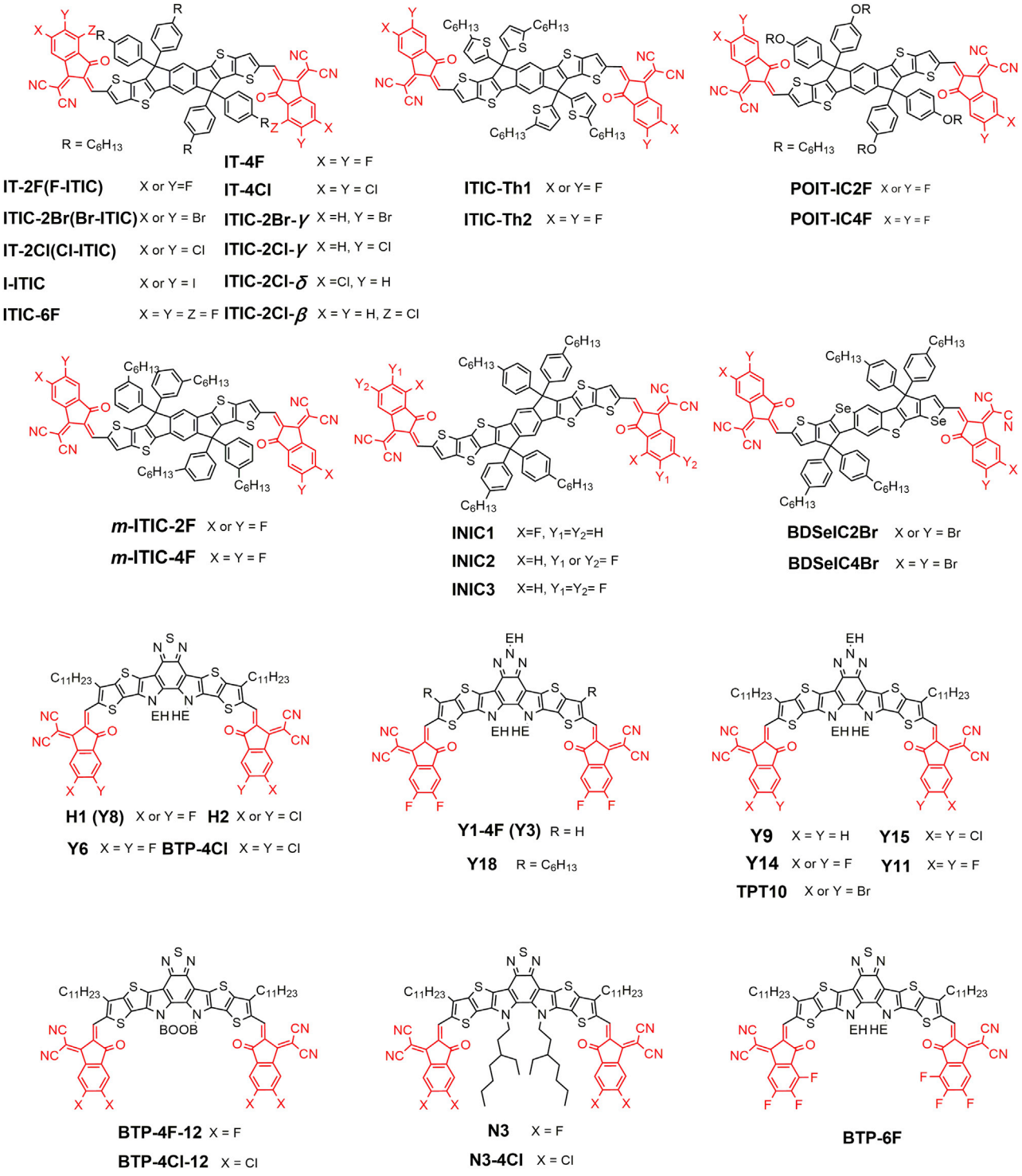

Figure 4. Chemical Structures of FREAs Based on Halogenated IC

IC Group with Halogen Substitution

Halogenation has been regarded as the most effective method to modify the IC group in the past few years (Figure 4). Halogen atoms show a weak electron-withdrawing inductive effect and relatively small atom size. In general, the introduction

of halogen atoms in EGs, especially in the fourth and fifth positions, can effectively strengthen the electron-withdrawing ability without affecting the planarity of EGs. For FREAs, halogenation of EGs can increase the ICT effect and downshift the LUMO level, as well as improving the crystallinity of the acceptor because of the non-covalent interaction between X···H and X···S. Correspondingly, halogenated FREAs usually exhibit a decreased V_{OC} but higher J_{SC} than their non-halogenated counterparts.

Hou and coworkers reported an ITIC derivative (IT-4F) based on dual-fluorinated IC.[58,59,130] IT-4F has broader absorption and a higher absorption coefficient than ITIC, which promotes photon harvesting. PBDB-TSF: IT-4F-based devices exhibit smaller energy losses ($E_g^{opt} - eV_{OC}$) of 0.66 eV than PBDB-T: ITIC-based devices (0.69 eV). PCEs of 13.1% and 13.7% were achieved on the basis of PBDB-T-S-F: IT-4F and PM6: IT-4F. The energy levels from ITIC to IT-*n*F (where n = 2–4) are decreased with the increasing number of fluorine atoms. The same trends are observed with INIC (INIC1, INIC2, INIC3),[61] ITIC-Th (ITIC-Th1, ITIC-Th2),[62] POIT-IC (POIT-IC2F, POIT-IC4F),[63] and *m*-ITIC (*m*-ITIC-2F, *m*-ITIC-4F).[64] In the INIC series, INIC3 exhibits red-shifted absorption, downshifted frontier orbital levels, and higher electron mobility. The FTAZ/INIC3 blend exhibits stronger crystallinity than its counterparts and maintains both materials' semicrystalline packings, possibly because of fluorine-induced intermolecular interactions. Despite a low V_{OC} of 0.852 V, FTAZ: INIC3 exhibits a high PCE of 11.5%, together with a J_{SC} of 19.68 mA/cm^2 and FF of 0.69. Fluorination has also been applied to Y-series. Y8/Y6 were obtained by mono/dual-fluorinating the IC group in Y5.[105,131] The optical bandgaps of Y-series are gradually reduced with the increased fluorine numbers. Compared with devices based on nonfluorinated Y5, fluorinated Y8- and Y6-based devices exhibited higher J_{SC} due to the red-shifted absorption. More reasonable phase separation in Y8 and Y6 device help achieve a higher FF. Consequently, PM6: Y6 exhibits a PCE of 15.7% with a V_{OC} of 0.83V and a J_{SC} of 25.3 mA/cm^2. A similar phenomenon is observed in Y1 and Y1-4F,[106] and the group of Y9, Y14, and Y11.[107,108,132] Xu et al.[109] designed a series of NFAs BTP-XF using IC-XF (where X = 0, 2, 4, or 6) as EGs. According to the computational data, fluorine atoms in BTP-XF increase the electrostatic potential (ESP) values of the conjugated surfaces and thus enhance intermolecular interactions with PBDB-TF, which leads to improved CT ratios in the lowest excited state. The increased CT ratio facilitates the charge separation and thus improves J_{SC}. It decreases EQE_{EL} and thus increases $E_{loss}^{non-rad}$ and V_{OC} loss. Because of the balanced V_{OC} and J_{SC}, BTP-4F demonstrated a higher PCE of 16.7% along with the polymeric donor PBDB-TF compared with BTP-0F, BTP-2F, and BTP-6F. All these findings demonstrate that fluorination of the IC EGs would decrease V_{OC} to some extent, which can be easily offset by the greatly improved J_{SC} and FF through proper D/A match.

Compared with fluorinated IC, chlorinated and brominated IC have more facile and economical synthesis routes by skipping the low-yield fluorination step, which will benefit future large-scale production and industrialization. Although chlorine exhibits lower electronegativity (3.16) than fluorine (3.98), the $3d_0$ orbital of Cl can delocalize the electron in the conjugation system. As a result, the Cl substituent shows stronger electron-withdrawing ability than F, as does Br. Several studies of chlorination and bromination of IC termini have been reported.[68,133–135] Consider IT-4Cl with dual-chlorinated IC as an example. The significant dipole moment of the C-Cl bond enhances the ICT effect and effectively extends the absorption of IT-4Cl to the NIR region.[65] Compared with IT-4F, IT-4Cl achieves a higher PCE of 13.45%, together with a lower V_{OC} due to the downshifted LUMO (−4.09 eV)

and a higher J_{SC} due to the red-shifted absorption in PBDB-T-2F-based OPV. The case of BDSeIC, BDSeIC2Br, and BDSeIC4Br well illustrates the effects of bromination on IC.[66] Compared with the nonbrominated acceptor (BDSeIC), BDSeIC2Br and BDSeIC4Br exhibit downshifted frontier orbital levels, stronger absorption in the range of 500–900 nm, stronger crystallinity, and enhanced electron mobility. PM6: BDSeIC2Br achieves a PCE of 12.5% with a relatively low E_{loss} of 0.52 eV, much higher than PM6: BDSeIC (PCE = 7.1%) and PM6: BDSeIC4Br (PCE = 9.6%).[66]

Interestingly, for Y-series FREAs, FREAs with chlorinated IC can achieve higher V_{OC} than their fluorinated counterparts despite the lower LUMO of the chlorinated FREAs. For instance, Y15 featuring the triazole core and chlorinated IC end group exhibits a much higher V_{OC} of 0.87 V than its fluorinated counterpart Y11 (0.83 V) along with PM6, although Y11 exhibits a higher LUMO of −3.93 eV than Y15 (−4.01 eV).[110,132] Similarly, BTP-4Cl, BTP-4Cl-12 and N3-4Cl show higher V_{OC} values of 0.867, 0.858, and 0.852 V than their fluorinated counterparts Y6 (0.834 V), BTP-4F-12 (0.855 V), and N3 (0.837 V), respectively.[112,113] This is attributed to the fact that FREAs based on chlorinated IC have a higher EQE_{EL} and thus a lower $E_{loss}^{non-rad}$ than their fluorinated counterparts for OPVs.[42,111]

Some groups have systematically compared FREAs based on F-, Cl-, Br-, and I-substituted IC units.[136–138] With the atomic weight of the halogen increased, the absorptions of halogenated acceptors are red-shifted, and their optical bandgaps are narrowed. Additionally, Li and coworkers found that Cl, Br, and I can improve the crystallinity of FREAs and charge transport due to the "heavy-atom effect."

Benefiting from the NIR absorption, halogenated FREAs show potential application in transparent devices and tandem devices. Li et al.[67] reported a 1.3 eV-E_g chlorinated FREA (BT-CIC) with a PCE of 11.2% ± 0.4%, J_{SC} of 22.5 ± 0.6 mA/cm^2, V_{OC} of 0.70 ± 0.01 V, and FF of 0.71 ± 0.02 in PTB7-Th based OPV. This NIR OPV exhibits EQE up to 75% between 650 and 850 nm while leaving a transparency window between 400 and 650 nm. The semitransparent OPV with a 10-nm-thick Ag cathode delivers a PCE of 7.1% ± 0.1%, with an average visible transmittance (AVT) of 43% ± 2%. Besides, the semitransparent device exhibits Commission d'Eclairage chromaticity coordinates of (0.29, 0.32) and a color rendering index of 91 for the simulated AM 1.5G irradiation transmitted through the cell. With a 30 nm Au cathode, PTB7-Th: IEICO-4Cl semitransparent device obtained a PCE of 8.38% and an AVT of 25.6%.[133] NIR-absorbing systems (e.g., PTB7-TH:IEICO-4F) can work as the rear subcell of the tandem device.[69,139–142]

Thienyl-Fused IC Group

Phenyl is the IC group can be replaced by a thienyl to construct the TC unit. The S-S interaction induced by thienyl can improve π-π stacking and crystallization (Figure 5). A group of isomeric EGs with different thienyl positions have been reported: *γ-TC* with 3, 4-position fused and β-TC (S atom on the carbonyl side) and α-TC (S on the other side) with 2, 3-position fused.[143–146] The thienyl positions can also affect the optoelectronic properties of FREAs. Compared with ITIC, ITCC (ITCT) with β-TC exhibits blue-shifted absorption and an upshifted LUMO level of −3.76 eV.[70,71] On the contrary, ITTC (ITCPTC) with γ-TC termini displays red-shifted absorption and a downshifted LUMO level of −3.96 eV.[72,147]

Further modifications, such as alkylation and halogenation, have also been used. For example, ITCC-M was designed by methylating the β-TC termini in ITCC.[73] ITCC-M (−3.67eV) exhibits higher LUMO levels than ITCC (−3.76 eV) and a 50 nm blue-shift

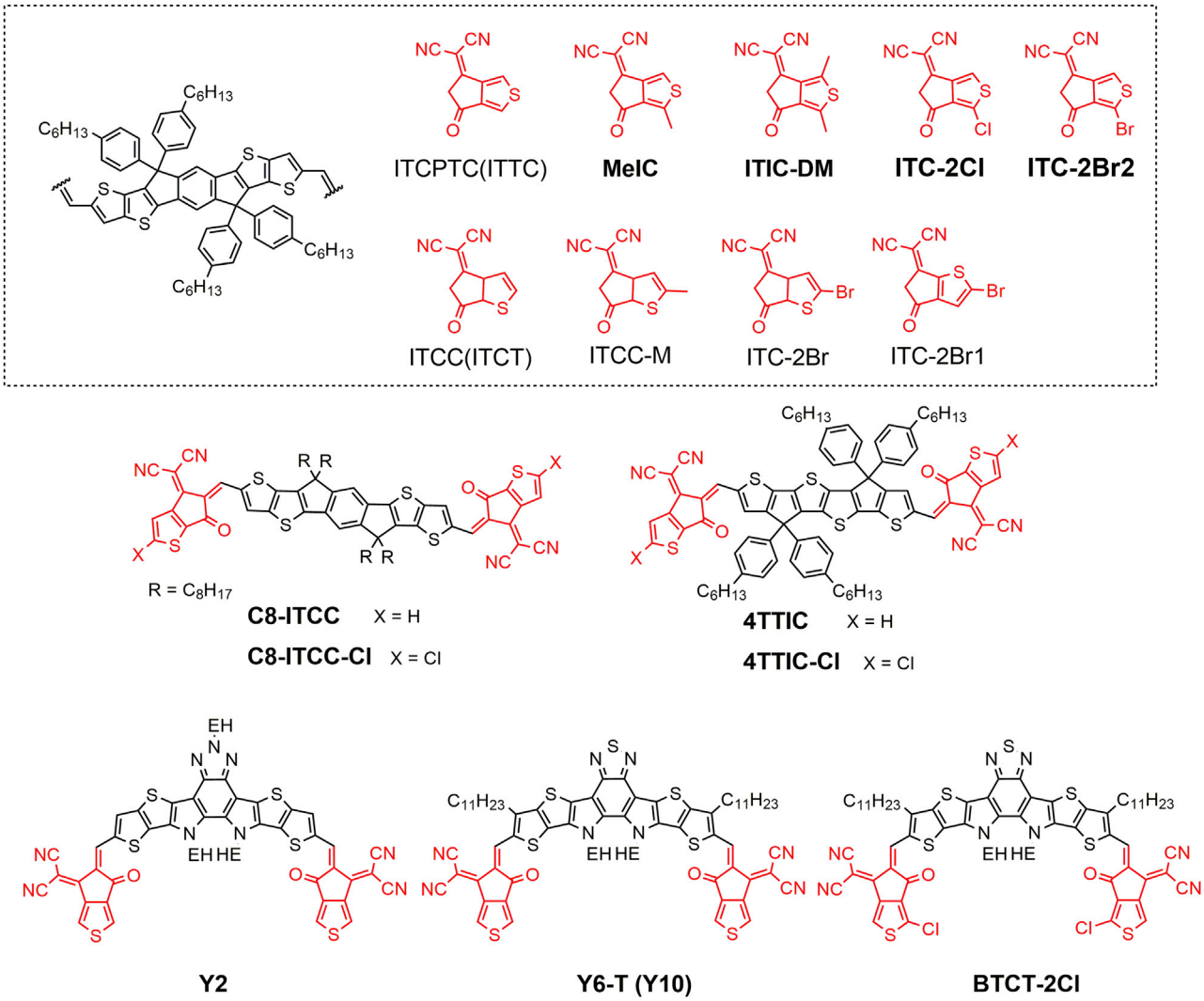

Figure 5. Chemical Structures of FREAs Based on Thienyl IC

of absorption onset. When blended with PBDB-T, ITTC-M shows a higher V_{OC} of 1.03 V, a lower J_{SC} of 14.8 mA/cm^2, and a PCE of 10.1% compared with ITCC (1.01 V, 15.9 mA/cm^2, and 11.4%, respectively). More important, benefiting from blue-shifted absorption and the high V_{OC} of PBDB-T: ITCC-M system, the tandem OPV device based on PBDB-T: ITCC-M as the rear subcell and PBDTTT-ET: IEICO as the front subcell achieves an impressive PCE of 13.8% with a V_{OC} of 1.80 V, J_{SC} of 12.0 mA/cm^2, and FF of 0.639. For γ-TC termini, 2, 5-positions in thienyl can be substituted.[148] MeIC and ITCT-DM are based on IDTT core and the mono-/dual-methylated γ-TC group from the parent ITCPTC bearing γ-TC, respectively.[74,75] TC unit-based ITCPTC, MeIC, and ITCT-DM exhibit continuously upshifted energy levels of −5.62/−3.96 eV, −5.57/−3.94 eV, and −5.48/−3.90 eV as well as gradually blue-shifted absorption (785, 784, and 783 nm), which show a similar tendency to IC unit. Along with polymeric donor (PBDB-T), ITCPTC, MeIC, and ITCT-DM exhibit V_{OC} values of 0.850, 0.896, and 0.904 V and J_{SC} values of 17.8, 18.07, and 17.4 mA/cm^2.[149,150] Among these, MeIC exhibits the highest efficiency of more than 12%, with a high FF of more than 0.74. Chlorine was introduced in β-TC in

the parent C8ITCC to construct C8ITCC-Cl.[76] C8-ITCC-Cl exhibits red-shifted absorption and downshifted frontier orbital levels than its nonchlorinated counterpart (C8-ITCC), as the chlorine atom has strong electron-withdrawing nature. Moreover, the noncovalent interactions induced by chlorine improve lamellar and π-π stacking of C8-ITCC-Cl, leading to higher electron mobility of $6.6 \times 10^{-4} cm^2 \cdot V^{-1} \cdot S^{-1}$ and FF of 0.73 of PBDB-TF: C8-ITCC-Cl devices. Therefore, C8-ITCC-Cl exhibits a higher PCE of 12.7% compared with C8-ITCC (10.8%). The same chlorination effect is reflected in the group of 4TTIC and 4TTIC-Cl.[77] Compared with ITTC, ITC-2Cl based on chlorinated γ-TC and IDTT core features a small E_g^{opt} of 1.58 eV with a low-lying LUMO. Cl atom in the end group increases the molecular packing. ITC-2Cl obtained a boosted PCE of 13.66% with a low V_{loss} of 0.67 V.[78] Luo et al.[79] systematically studied the impact of bromination on end groups and FREAs. They introduced Br into three isomeric TC end groups, CPTCN-Br (2-position of β-TC), CPTCN-Br1 (3-position of α-TC), and CPTCN-Br2 (2-position of γ-TC), and obtained three FREAs: ITC-2Br, ITC-2Br1, and ITC-2Br2. For ITC-2Br and ITC-2Br1, the EG conformation and the bromine position have little impact on material properties such as energy levels and photovoltaic performance. However, ITC-2Br2 features a smaller E_g^{opt} of 1.59 eV (ITC-2Br of 1.73 eV and ITC-2Br1 of 1.70 eV). A high J_{SC} of more than 19 mA/cm^2 and FF of 0.74 were enabled by board absorption and high crystallinity of the PBDB-T-2F: ITC-2Br2 system.

Thienyl IC and its derivatives also showed great potential in Y-series FREAs. Y2 was designed by replacing phenyl with thienyl.[40] Y2, based on γ-TC, exhibits a strong ICT effect with a red-shifted absorption. The electron-deficient ability of γ-TC is stronger than that of IC but weaker than that of 2F-IC. The E_g^{opt} value of Y2 (1.40 eV) is between Y1 (1.44 eV) and Y1-4F (1.3 eV). Y2 displays a higher J_{SC} versus a lower V_{OC} compared with Y1. A similar tendency is observed in Y5, Y10 (Y6-T), and Y6 systems.[116,151] BTCT-2Cl is obtained by fluorinated TC units in Y6-T.[117] BTCT-2Cl exhibits downshifted HOMO and LUMO, which is similar to ITIC series. Other aromatic nuclei, such as furan, pyrrole, thiazole, and iminazole, can be considered as substitutions of the benzene ring in IC EGs, offering more possibilities for FREAs.

π-Extended IC Group

Intermolecular π-π interactions are likely to occur primarily between the EGs of considerably slipped neighbors, which have the highest LUMO coefficients. Enlarging the π-conjugation of termini can improve the stacking of termini and facilitate charge transport (Figure 6).[152–154] Li et al.[80] designed IDTN by extending the phenyl to naphthyl in IC EGs of IDTIC. The extended termini delocalize the π-electrons of LUMO, while HOMO is confined in the IDTT core, resulting in a decreased LUMO and a similar HOMO. Because of the π-conjugation extension by fusing two phenyls, IDTN exhibits stronger molecular aggregation, more ordered packing and thus distinctively higher electron mobility than IDTIC. The PBDB-TF: IDTN system exhibits higher PCE of 12.2% and FF of 0.78 compared with the PBDB-TF: IDTIC case (PCE = 7.4%, FF = 0.57). Marks and coworkers reported IT(z)N-CX, a family of π-extended IDTT-based NFAs with naphthalene-fused termini, wherein ITN-C9 and ITzN-C9 are isomers with different naphthalene-fused end groups. Compared with ITN-C9, ITzN-C9 shows significantly blue-shifted absorption and an elevated LUMO energy level. For ITN-C9 and ITzN-C9, single-crystal structures indicate that the LUMO-rich termini have intermolecular π-π distances as short as 3.31 A in vertical columns, electronic coupling integrals as large as 38 meV, and internal reorganization energies as small as 0.133 eV. Therefore, ITN-C9 and ITzN-C9 exhibit high mobilities (10^{-4} $cm^2 \cdot V^{-1} \cdot s^{-1}$). The optimal PCE of 9.33% is achieved by the as-cast PBDB-TF: ITN-C9 blends, while the PBDB-TF: ITzN-C9 blend requires

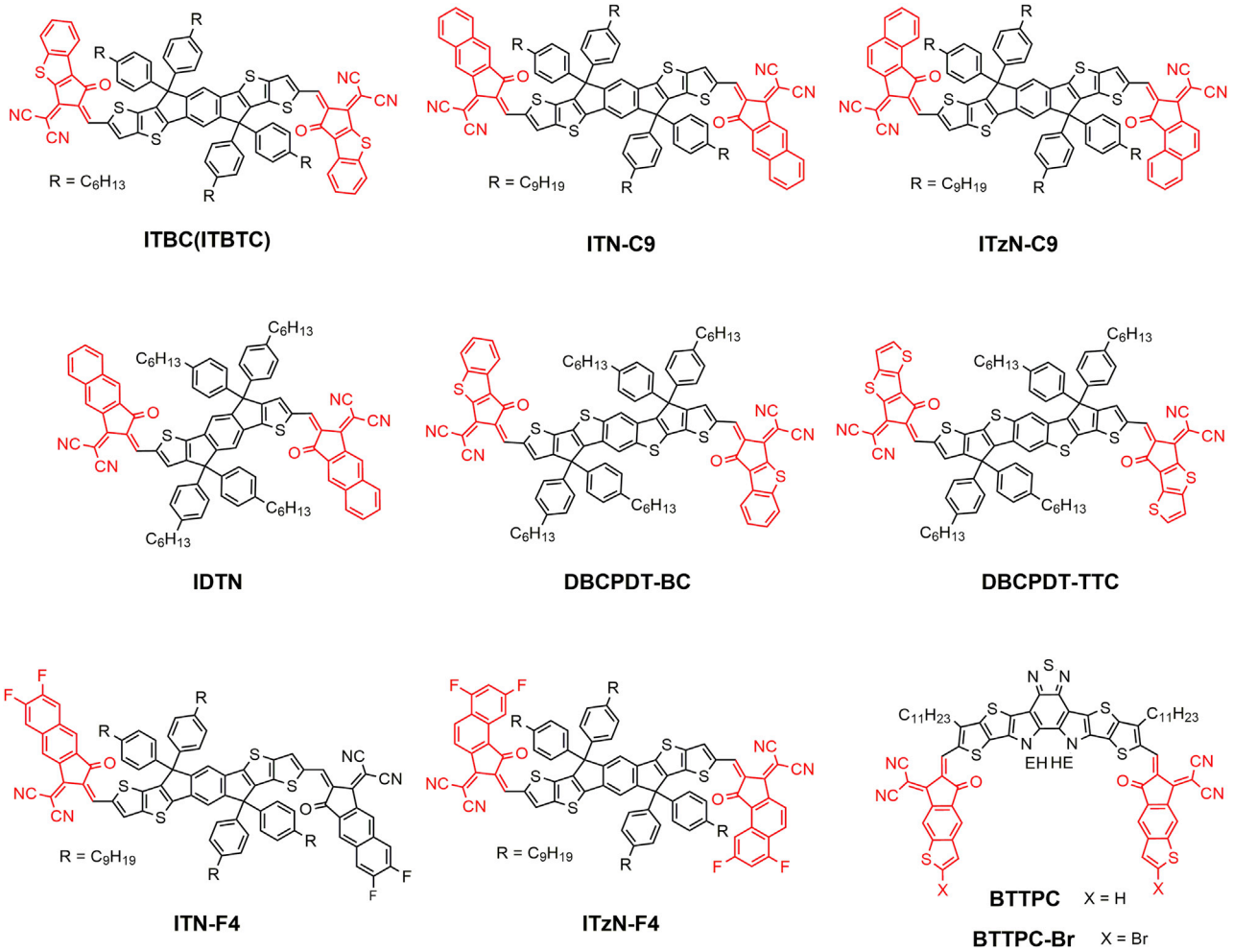

Figure 6. Chemical structures of FREAs based on π-extension IC

thermal annealing at the acceptor cold crystallization temperature to deliver 9.51% efficiency.[81,155] Notably, the π-extension to naphthyl would reduce the solubility of the acceptor because of its strong crystallinity. To ensure the solution process, FREAs with naphthalene-fused termini should be modified to increase solubility by elongating the alkyl chain or reducing the conjugation.[80,154,156]

π-Extension of IC EGs has also been reported by replacing phenyl in IC with benzothienyl (BTC). Compared with phenyl-fused ITIC, ITBTC featuring conjugation-extended benzo[b]thiophene-fused termini exhibits decreased electron-pulling strength of the termini and stronger intermolecular interactions of FREAs.[82,83] Consequently, ITBTC exhibits an elevated LUMO, higher electron mobility, and more favorable active layer morphology. On the basis of the same IDTT core, the absorption and LUMO level of ITBTC film locate between those of ITIC (with IC termini) and ITCC (with β-TC termini). More important, ITBTC shows a distinct enhancement of absorption in the range of 320–570 nm relative to ITIC and ITCC. Although ITBTC displays slightly blue-shifted absorption than ITIC, ITBTC induces the extra absorption band in the short-wavelength range by its benzo[b]thiophene termini and exhibits a higher J_{SC}. Benefiting from these characteristics, ITBTC achieves a PCE of 10.29%, together with a V_{OC} of 0.94V and FF of 0.713, exceeding ITIC (PCE = 9.53%).

An alternative π-extension method is replacing phenyl in IC with thienothiophene.[152] The electron-rich TT moiety decreases the electron-accepting strength, thereby elevating the HOMO and LUMO. The extended conjugated bicyclic TT ring beneficially induces an additional optical transition at short wavelengths. The TTC end group is paired with a heptacyclic ladder-type core (BDCPDT) to construct a FREA BDCPDT-TTC, which exhibits a shallower HOMO and LUMO than its counterpart BDCPDT-IC. The PBDB-T: BDCPDT-TTC device delivers an improved PCE of 10.29%, with simultaneously enhanced V_{OC} of 0.94 V and J_{SC} of 17.72 mA/cm^2 in relative to the PBDB-T: BDCPDT-IC device (9.33%).

Further halogenation can be applied to π-extended EGs. ITN-F4 and ITzN-F4 were obtained by fluorinating ITN-C9 and ITzN-C9, respectively.[85] ITN-F4 and ITzN-F4 have been found to provide higher PCE and lower internal reorganization energy (λ_{INT}) and increased electronic coupling than their non-π-extended and non-fluorinated counterparts when paired with PM6. This indicates that the strategy of π-extension and halogenation could be used in tandem to strengthen π-π stacking and facilitate charge transport.

Exchanging the position of phenyl and thienyl in BTC termini affords the TPC EGs. BTTPC and BTTPC-Br are obtained by replacing the benzene ring in IC of Y5 with benzothiophene and bromobenzothiophene, respectively.[118] In the presence of a similar or even smaller HOMO offset, PBDB-T: BTTPC-Br and PBDB-T: BTTPC blends exhibit efficient hole transfer from the acceptor to the donor, 4 and 1.5 times faster than PBDB-T: Y5 blend. BTTPC-Br and BTTPC show PCEs of 15.22% and 14.51% compared with 13.78% for Y5 with PBDB-T as the donor.

Other Types of IC-Based EGs

Several works have explored the concurrence of different halogens or alkyls in termini (Figure 7). Wan et al.[86] designed a hybrid dihalogenated IC (IC-BrCl), with one Br atom and one Cl atom simultaneously grafted to an IC skeleton. Compared with its chlorinated and brominated counterparts, BDSe-2(BrCl) with IC-BrCl termini exhibits the same E_g^{opt} of 1.39 eV. The crystallinity of the acceptors was progressively improved, and their miscibility with PM7 was gradually reduced with increasing Br numbers. The PM7: BDSe2(BrCl) system exhibits the strongest face-on orientation, the most reasonable phase separation scale, the highest and most balanced carrier mobilities, and the weakest charge recombination because of an excellent balance of the miscibility and crystallinity of the blend film. Therefore, PM7: BDSe2(BrCl) OPVs exhibit an outstanding PCE of 14.5% with a high FF of 76.5%, outperforming PM7: BDSe-4Cl device (PCE = 13.8%) and BDSe-4Br device (PCE = 13.2%). Luo et al.[119] designed a series of dual-halogenated IC EGs by precisely manipulating the position of Cl and Br atoms (IC-ClBr, IC-ClBr1, and IC-ClBr2). Among them, the FREA BTP-ClBr based on IC-ClBr shows the highest PCE of 16.82%, with an outstanding FF of 0.79.

EGs can be modified with the marriage of methyl and halogen.[87,157] Yang and coworkers reported the new EG CFDCI, which is short for 5-fluoro-6-methyl-3-dicyanovinylindan-1-one. A prototype SMA ITCF bearing CFDCI EG demonstrates moderate crystallinity in pristine film and more balanced charge transport and reduced bimolecular recombination compared with IT-DM and IT-4F. Together with J71 donor, ITCF exhibits a PCE of 13.25% and FF of 78.8%, exceeding IT-DM and IT-4F with PCEs of 12.05% and 11.66%. The existence of methyl would improve charge transport but cause a high surface roughness. The F atom can strengthen the ICT effect and π-π stacking. The absorption spectra of ITCF are located closer to IT-4F

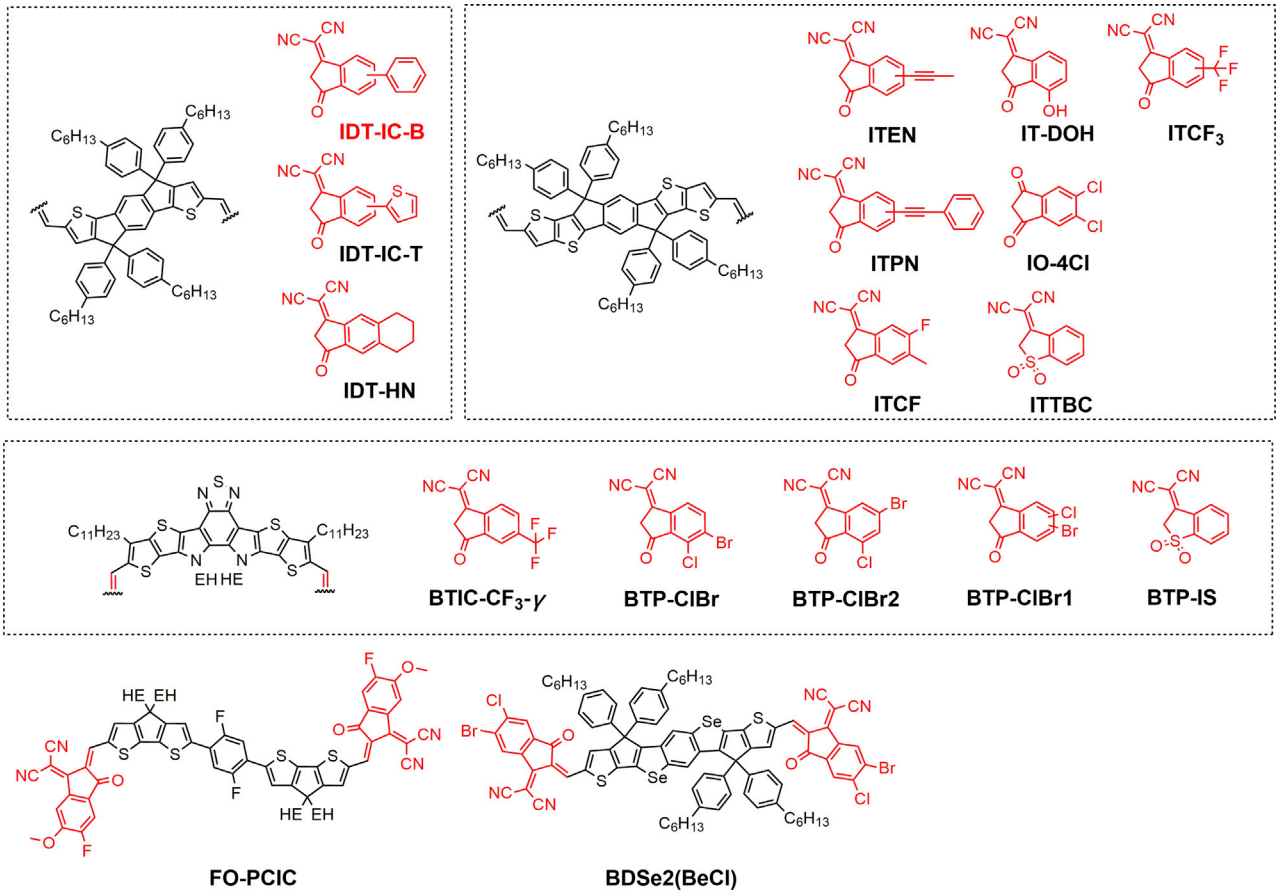

Figure 7. Chemical Structures of FREAs Based on Other Types of IC Derivatives

rather than IT-DM, which is a benefit to the J_{SC}. Methoxyl and fluorine are also selected to co-modify the IC group.[89]

Besides the aforementioned thienothiophene, naphthalene, and benzothiophene fused end group, thienyl and phenyl as small electron-donating aryls can be linked with IC by a single bond to construct new termini. This strategy extends the conjugation length and twists the flanking termini simultaneously. Such a twist can control charge transport and film morphology, and the extended conjugation increases the connectivity of FREAs and thus enhances the electron mobility. IDT-IC-T featuring thiophene substituted IC and IDT-IC-B featuring benzene substituted IC are designed on the basis of the parent IDT-IC. IDT-IC-T exhibits a smaller twist angle of 20° between aryl and IC and tighter π-π stacking relative to IDT-IC-B. IDT-IC-B- and IDT-IC-T-based blends present finer phase separations than that of IDT-IC. Ultimately, IDT-IC-B and IDT-IC-T demonstrate much higher PCEs of 8.72% and 9.43% than IDT-IC (5.82%).[88] Phenyl can also be linked with IC by a triple bond to design a phenylethynyl-substituted EG. ITPN shows smaller binding energy and reorganization energy to ITIC and the ethynyl-substituted acceptor (ITEN), ascribed to the extended π-conjugation and the rotatability of phenylethynyl end groups.[90] ITPN exhibits stronger molecular aggregation, more ordered packing, and thus enhanced charge transport. Along with PBDB-TF, ITPN yields a higher PCE of 12.6% compared with ITEN and ITIC.

The HN-IC end group is obtained by introducing cyclohexane into the benzene unit of IC group.[91] Compared with IDT-IC bearing IC termini, IDT-HN exhibits a higher LUMO because of the electron-donating ability of cyclohexane, and broadened and intensified absorption is attributed to the stronger intermolecular interactions between the end groups. Along with PBDB-T, IDT-HN exhibits a higher PCE of 10.22%, with simultaneously improved V_{OC}, J_{SC}, and FF, compared with IDT-N (PCE = 8.89%) and IDT-IC (PCE = 6.11%).

The hydroxyl group is also introduced into the IC EGs, as it can potentially form strong intermolecular hydrogen bonds to improve molecular arrangement.[92] IT-OH and IT-DOH exhibit slightly smaller bandgap and red-shifted absorption, ascribed mainly to the H-bond between hydroxyl and carbonyl. IT-DOH and IT-OH therefore exhibit more ordered molecular packing than their counterpart (ITIC). By comparison with ITIC, the trifluoromethylated ITCF3 exhibits deeper energy levels, stronger and red-shifted absorption, and better electron transport. Because sp^3 hybrid CF_3- has a larger size than H atom, ITCF3 shows weak lamellar stacking but tighter π-π stacking than ITIC. Better phase separation, stronger π-π stacking, and more predominant face-on orientation are observed in the PM6: ITCF3 blend. Correspondingly, OPV devices based on PM6: ITCF3 show a much higher PCE of 13.3% (V_{OC} = 0.84 V, J_{SC} = 20.9 mA/cm^2, FF = 0.76), much higher than non-fluorinated ITIC-based OPVs (PCE = 8.4%).[93]

Replacing the carbonyl in IC with sulfonyl (BC) was also investigated. ITTBC and ITThBC were synthesized by end-capping IDTT and IDTT-Th with BC.[94] Because of the stronger electron-pulling ability of sulfonyl, these two acceptors show deeper energy levels and slightly red-shift absorption compared with ITIC. PCEs of 6.89% and 7.59% are achieved in ITTBC and ITThBC devices, which is lower than that of ITIC.[158] The same EGs were used with an end-capping Y-series core and obtained BTP-IS with a PCE of 12.79%.[122] The low performance may be attributed to the sp^3-hybrid-like S atom, which forms a tetrahedron structure unfavorable for π-π stacking of EGs.

Simple 1,3-indanedione is also used as an EG. IO-4Cl has a weaker ICT effect and a larger E_g^{opt} compared with IT-4Cl.[95] PBDB-TF: IO-4Cl shows a PCE of 9.80% under AM 1.5G illumination (100 mW/cm^2) with a high V_{OC} of 1.24 V. Benefiting from the proper absorption for indoor light conditions, IO-4Cl shows an outstanding PCE of 26.1% with 1 cm^2 active area under a 2,700cK LED lamp at 1,000 lux. Moreover, this device exhibits high stability under continuous illumination of LED for 1,000 h. The thickness insensitivity would benefit large-scale fabrication. Considering the UV stability issue of organic semiconductors, it might be feasible for OPVs to serve as an indoor power source as a low-hanging fruit. A similar strategy is applied to parent BTP-4Cl to obtain ZY-4Cl.[121] ZY-4Cl with 1,3-indanedione exhibits a wider bandgap and an obvious 100 nm blue-shifted absorption. More important, when blended with P3HT, ZY-4Cl shows a record-high PCE of 9.46% for P3HT-based OPV with a V_{OC} of 0.88 V, J_{SC} of 16.49 mA/cm^2, and FF of 0.65. The P3HT: BTP-4Cl system exhibits only 1.01% PCE.

Asymmetric Substitution

ADA- and A-DA¢D-A-type FREAs usually use a symmetric configuration with the same EG at both ends. For symmetric FREAs, increasing the J_{SC} by red-shifting the absorption would always be accompanied by the reduction of V_{OC}, and vice versa. Several works have explored the asymmetric EG strategy (Figure 8). Compared with nonpolar symmetric molecules, asymmetric FREAs with different

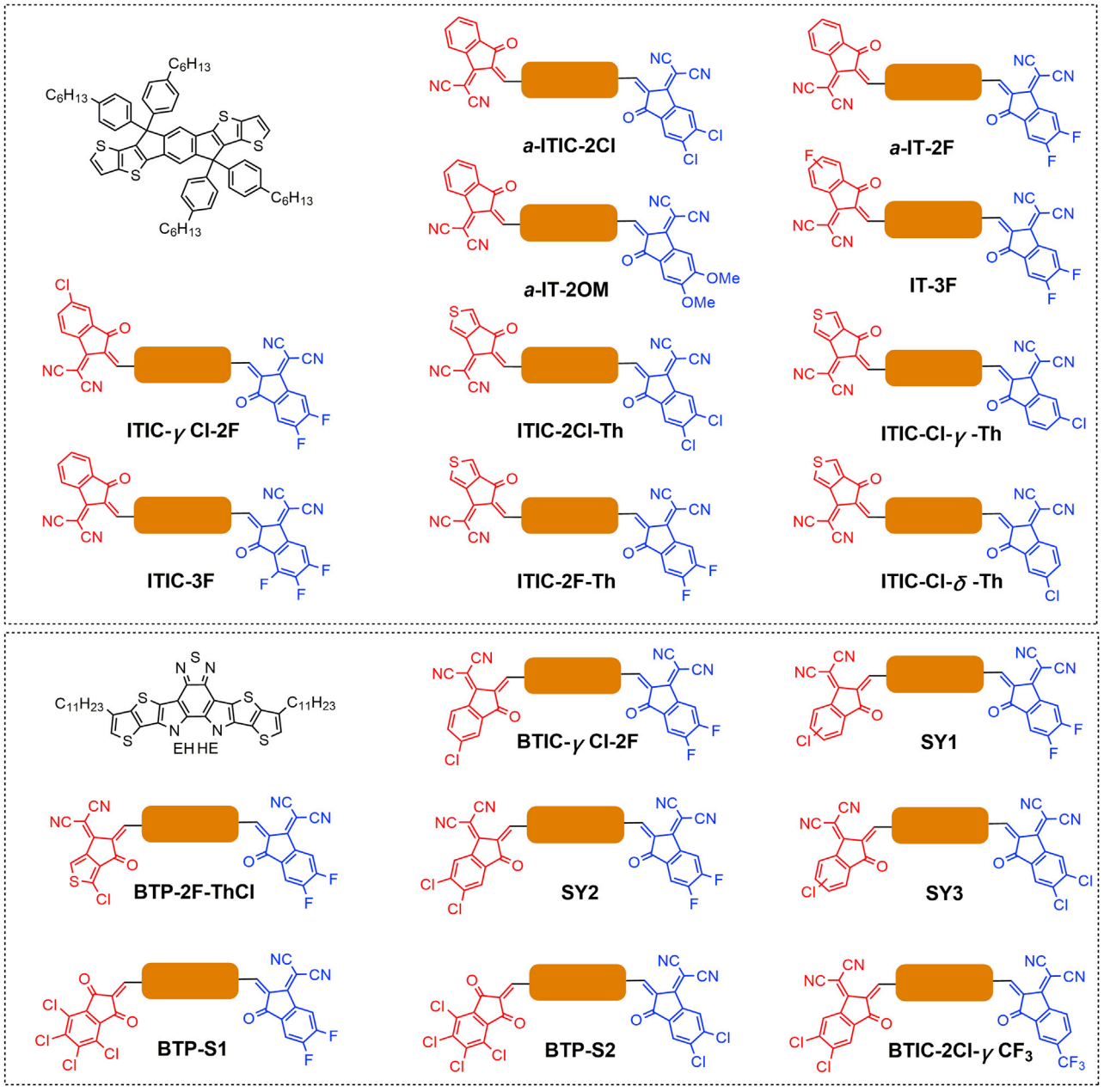

Figure 8. Chemical Structures of FREAs Based on Asymmetric Substitution

EGs realize a permanent dipole moment, which strengthens the intermolecular interaction and achieves more ordered molecular orientation.[96] Such a dipole moment enabled by the A_1-D-A_2 structure can also tune the crystallization and other charge carrier behaviors. Moreover, the extra selective EGs can fine-tune the energy levels to reduce the energy loss and ensure charge separation. In addition, the strategy of asymmetric EGs is more feasible and low cost compared with constructing asymmetric fused-ring core. α-IT-2F and α-IT-2OM are the first attempts to investigate the A_1-D-A_2 strategy. α-IT-2OM with y axis-paralleled dipole moment shows an intensive bimolecular binding, which promotes molecular packing and facilitates charge transport. Finally, devices based on PBDB-T: α-IT-2OM show a higher PCE

of more than 12% with an improved V_{OC} of 0.93 V, J_{SC} of 18.11mA/cm^2, and FF of 0.72, compared with PBDB-T: ITIC devices with a PCE of 9.53%. Such an effect also works in thick-film devices, with PCEs of 11% at 200 nm and 9% at 450 nm. The asymmetric FREA bearing IC and dual-chlorinated IC end groups (*a*-ITIC-2Cl) is designed from the symmetric FREA with mono-chlorinated IC (ITIC-2Cl-β). The asymmetric *a*-ITIC-2Cl shows a lower LUMO (−3.77 eV) than ITIC-2Cl-β (−3.71 eV) and exerts a larger dipole moment, contributing to electron transport. Moreover, *a*-ITIC-2Cl forms a 3D interpenetrating network with shorter π-π distances and better molecular planarity than ITIC-2Cl-β with linear packing. Consequently, *a*-ITIC-2Cl exhibits a PCE of >12%, ∼10% higher than ITIC-2Cl-β.[97] Other different EGs were combined to achieve A_1DA_2 asymmetric FREAs, such as IDTT-2F-Th, ITIC-Cl$^-$δ-Th, ITIC-Cl$^-$γ-Th, and ITIC-2Cl-Th.[99,159]

Recently, asymmetric strategies have also been applied to Y-series FREAs. For instance, BTP-S1 and BTP-S2 are synthesized on the basis of one EG of 4,5,6,7-tetrachloroindane-1,3-dione (I-4Cl) and another one of 2F-IC or 2Cl-IC.[123] Despite the four Cl atoms in I-4Cl, the removed malononitrile unit reduces the ICT effect. By comparing BTP-S1 and Y6, the disappearance of malononitrile slightly weakens π-π stacking. BTP-S2 with its C-12 side chain retains the π-π stacking distance of Y6. Along with PM6, BTP-S2 reveals an EQE_{EL} 5 times higher than Y6, which indicates the smaller non-radiative loss of PM6: BTP-S2. On the basis of BTP-S2, the binary and ternary devices achieve PCEs of 16.37% and 17.43%, respectively. Liu et al.[124] designed three asymmetric FREAs on the basis of 1Cl-IC/2F-IC (SY1), 2Cl-IC/2F-IC (SY2), and 1Cl-IC/2Cl-IC (SY3) EGs. On the basis of the same backbone, all three acceptors display exciting efficiency of more than 16%. SY1 shows a higher LUMO level compared with symmetric molecules such as Y6 and Y6-Cl. Moreover, this modification has little negative influence on absorption or phase separation and thus retains high J_{SC} and FF. As a result, the PM6: SY1 device shows a high PCE of 16.83%. BTP-2F-ThCl is another typical example of asymmetric FREAs.[125] When end-capped with BTP core, γCl$^-$TC could improve V_{OC} by its lower electron-deficient ability compared with 2F-IC, while the large energy level offset of PM6: BTP-2ThCl caused the unfavorable energetic alignment and inefficient charge separation. Moreover, for PM6: Y6, CT state dissociation is large enough to achieve CT, which implies that the LUMO level could be further improved with high efficiency.[160] Replacing one of the 2F-ICs in Y6 with γCl$^-$TC improves V_{OC} from 0.84 to 0.87 V without blue-shifting absorption. Finally, the PM6: BTP-2F-ThCl system realizes a PCE of more than 17%. A similar strategy has also been applied to form BTIC-2Cl-γCF_3 and achieve a PCE of 16.31%.[126] With these successes, considering a large quantity of EGs, the asymmetric strategy can be furtherly used to optimize the performance.

Impact of IC EGs on Blend Film Morphology

The morphology of the OPV active layer is vital for device performance. The morphology issue in BHJ OPVs refers mainly to the phase separation in blending films, accompanied by the roughness of the top surface. Percolated and continuous phase separation is required to avoid insufficient exciton dissociation and unbalanced charge transport.[161] For IC-based FREAs, self-aggregation and miscibility with the donor are two key fundamental factors for phase separation morphology. Because of their intermolecular π-π stacking, the IC EGs affect phase separation greatly. Here we concisely discuss the impact of IC EGs on film morphology.

One of the fundamental factors is FREAs' solubility, which is influenced by IC. For example, the methoxyl to butoxyl IC-based IT-O (1-4) exhibit decreased solubility with increased alkoxyl chain length. In this case, the PBDB-T/IT-O3, 4 show a

dramatically larger domain size. Such over-aggregation in IT-O3, 4-based devices leads to poor PCEs, lower than half of the IT-O1, 2-based devices' PCE.[57] Moreover, π-extension IC would also reduce the solubility of FREAs. ITN-C6, with the IC π-extension of ITIC, shows a very high surface roughness of 119 nm when blending with PBDB-T-TF. Devices based on this active layer system display a PCE lower than 0.1%.[81] Similar phenomena were reported by Li et al.[80] Such high roughness of the active layer top surface impedes the formation an ohmic contact with the transport layer above and causes large leak current and contact resistance.[162]

Unlike the ball-shaped FA, planar FREAs are required to form "face-on" orientation in relative to substrate to facilitate the charge transport.[163] π-Extension IC EGs can form more ordered and compact "face-on" stacking and orientation. For example, two-dimensional (2D) grazing incidence wide angle X-ray scattering (GIWAXS) shows that PBDB-TF: IDTN blends exhibit more preferentially "face-on" orientation than PBDB-TF: IDTI, because of the improved intermolecular interaction enabled by the larger IC EGs (IDTN).[80] A similar phenomenon is observed in FREAs with different types of π-extension IC EGs (e.g., ITBC, ITN-C9, BDCPDT-TTC).[81,83,84]

Miscibility between donor and acceptor is another key factor to tune the phase separation of blending films.[164] In a previous study, the Flory-Huggins interaction parameter (χ) was used to estimate the miscibility of two components in the blend. The high value of χ means low miscibility, and sometimes indicated high domain purity, and vice versa. By measuring the contact angle and calculating the surface tension (γ), impacts of IC EGs on χ and miscibility have been reported. For example, the types and positions of substitutes would influence the χ value between donors and FREAs and thus miscibility. The χ (»2.7) of the PBDB-T: IT-M blend is higher than that of the PBDB-T: IT-DM blend (»2.0) despite low solubility of IT-DM. Also, by varying the intermolecular interactions between PBDB-T and IT-OM, the larger χ for PBDB-T/IT-OM-4 can result in weaker mixing, in line with the more obvious phase separation observed experimentally. Generally, the fluorinated organics exhibit hydrophobic nature. However, within the fluorinated IC-based FREAs, IT-4F is more hydrophilic than IT-M, which leads to a 15 times larger χ of PBDB-TF:IT-4F than that of PBDB-TF: IT-M. Stronger crystallization was observed in halogenated IC-based FREAs (F-F, F-Cl, and F-Br) compared with F-H.[137] As a result, the F-F, F-Cl, and F-Br-based blend exhibits a more distinctive fibrillar network and stronger phase separation than its nonfluorinated counterpart.

Great efforts have been undertaken to build the relationship between phase separation and device performance. We have seen continuous improvement in morphology understanding over the history of OPVs. With the highly efficient materials under development, such as Y6-series, new insights will emerge to incorporate understanding of excitons' diffusion length and other issues through theoretical and experimental approaches.[165] The morphology of the highly efficient layer-by-layer/sequential deposition devices and super-thick devices (i.e., >1,000 nm) also needs further exploration.[166–171]

SUMMARY AND OUTLOOK

IC EGs have shown great potential in FREAs in the field of OPVs because of their synthesis simplicity and multi-modification, with ~18% PCE achieved. A PCE of more than 20% on the basis of IC-FREAs is widely expected in coming years. However, to achieve higher efficiency and longer lifetime of OPVs, and to establish a clear relationship among structure, properties, and performance,[172–174] key scientific issues must be taken into consideration, which we discuss below.

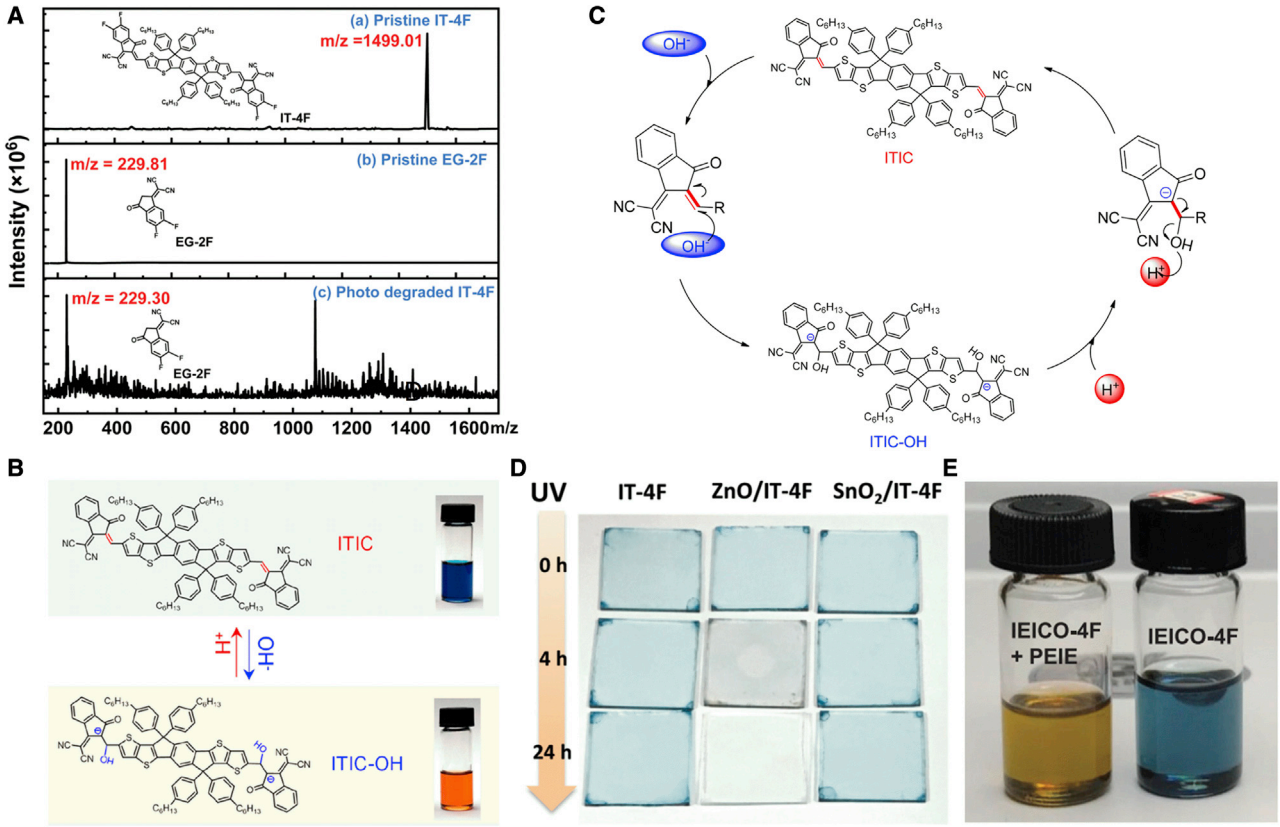

Figure 9. Chemical and Light Stability Issues of IC-Based FREAs

(A) MS spectra of pristine nonfullerene acceptor IT-4F (a), pristine acceptor moiety EG-2F (b), and photo-degraded IT-4F (c), respectively. Reprinted with permission from Jiang et al.[175] Copyright 2019 The Royal Society of Chemistry.

(B) Chemical structure and photograph of ITIC solutions in acid/basic surroundings. Reprinted with permission from Zhu et al.[176] Copyright 2019 American Chemical Society.

(C) Proposed mechanism of the reversible conversion of ITIC and ITIC-OH under acidic and basic conditions. Reprinted with permission from Zhu et al.[176] Copyright 2019 American Chemical Society.

(D) Pictures of IT-4F thin films on glass, glass/ZnO, and glass/SnO_2 substrates under continuous UV illumination (365 nm, 5 mW/cm^2) for different times. Reprinted with permission from Jiang et al.[175] Copyright 2019 The Royal Society of Chemistry.

(E) Photograph of IEICO-4F and IEICO-4F mixed with PEIE solutions. Reprinted with permission from Xiong et al.[177] Copyright 2019 Wiley-VCH.

Stability

Despite the exciting efficiency achieved, FREAs based on IC and its derivatives, such as ITIC, have chemical instability issues (Figure 9A).[175,176,178] ITIC will degenerate to ITIC-OH when encountering OH^-, as the nucleophile hydroxy anion will attack the double bond in the linkage between core and end groups (Figure 9B). The disintegration of the double bond breaks the molecule conjugation and eliminates the ICT effect, indicated by the total change of the solution color. The degeneration is a reversible process, with the double bonds in FREA molecules being recoverable in acid surroundings (Figure 9C). Note that classical interlayers such as ZnO and PEIE are basic, whereas PEDOT: PSS is acidic (Figures 9D and 9E). Direct contact of the FREA-based active layer with the basic interlayer would inevitably degrade device performance. In addition, ZnO can also be the photocatalyst to degrade FREAs. When IT-4F film deposited on ZnO was exposed to UV, it decomposed in a few hours. Replacing ZnO with SnO_2 nanocrystal is another effective way to improve the stability of FREAs because of the less photocatalytic nature of SnO_2.[175] Protonating PEIE by aqueous solution processing can deactivate N to NH^+, prevent it from reacting with the acceptor, and therefore improve stability.[177]

Substitution in IC EGs would also greatly influence stability. Du et al.[28] reported that the photo-stability of IT-M- and IT-DM-based OPV devices represented a serious concern. IT-DM-based devices retain only 10% of their initial PCE (20% of J_{SC} and 50% of FF) under continuous LED illumination over 1,600 h in N_2 atmosphere (O_2 below 0.5 ppm). *In situ* Fourier transform infrared (FTIR) measurements exhibit the degradation of acceptor with decreased absorption of C = C and C<u>O</u>N by photo-oxidation. The break of conjugation causes energetic traps that continuously decrease both J_{SC} and FF. In contrast, the fluorinated IC-based FREAs have intrinsic light stability against light soaking.[28] Devices based on PBDB-T: ITIC-2F (IT-4F) exhibit near 80% of the initial PCE over 11,000 h under equivalent 1 sun illumination in N_2 conditions.

Moreover, the mechanism of FREA photo-bleaching in ambient conditions has been systematically investigated with more than 30 FREAs.[179] Using FTIR and X-ray photoelectron spectroscopy (XPS), several possible reaction sites have been demonstrated: the C = C between the donor and acceptor units and the C = C on malononitrile or bithiophene in fused core and side chains. On the basis of the same IDTT backbone, the photo-bleaching rate of chlorinated IC acceptor is found to be lower than that of IT-4F, while alkylated and pristine IC exhibit quicker light oxidation. Notably, the photo-stability of Y-series FREAs is much better than that of ITIC series. Overall, the double bond between fused core and EGs is the most instable unit.

Although the initial research has provided important information on the understanding of the NFA OPV degradation, the intrinsic relationship between the chemical structure and stability of FREAs is still unclear and certainly deserves future exploration.

Isomerism

As mentioned earlier, the fourth and fifth positions in IC can be modified to improve performance. However, it has been found that the isomers exist in mono-substituted IC. For example, fourth-methyl IC and fifth-methyl IC with similar polarity can hardly be separated by column chromatography or recrystallization. Theoretically, the impurity can affect the properties of materials, as well as device performance, which is difficult to control and leads to batch-to-batch variation. The random composition of the isomer mixture would affect the molecular arrangement to a great extent. Compared with alkyl-substituted IC termini, alkoxyl substituted IC isomeric end groups are easier to separate because of polarity differences.

Like methyl substituent, the isomeric mono-fluorinated IC unit can hardly be purified because of the similar structure and polarity of 5- and 6-position fluorinated IC. Lai et al.[100] attempted to obtain pure mono-chlorinated and mono-brominated IC units. From 3 g IC-Cl-*m* isomer mixture, 0.5 g IC-Cl-γ is obtained by recrystallizing from ethanol and 1 g IC-Cl-δ from chloroform. Moreover, the remaining product could be recycled for the next recrystallization. Isomer-free ITIC-2Clγ shows good planarity and closed π-π stacking distance and constructs a 3D interpenetrating network that facilitates charge transport, while ITIC-2Clδ has only a linear stacked structure. ITIC-2Clγ shows a high PCE of 13.03% with improved V_{OC}, J_{SC}, and FF. Devices based on ITIC-2Clδ show a PCE of 11.5%. It is easy to understand that because of the disordered packing of the mixture, ITIC-2Cl*m* shows a PCE of only 10.85%, lower than two isomer-free FREAs. Similar work has been applied to brominated IC termini.[101] Compared with ITIC-2Br-*m* (a three-isomer mixture), purified ITIC-2Br-γ shows a high absorption coefficient in both solution and film. ITIC-2Br-

γ single-crystal analysis shows a similar 3D network with ITIC-2Clγ. The isomer-free ITIC-2Br-γ device shows a higher PCE than the ITIC-2Br-*m* counterpart.

In the Michael addition reaction, β-TC is the primary product because the conformation of α-TC is instable. As a comparison, the BTC IC can generate stable α-BTC. Moreover, isomer-free α-BTC can be purified through recrystallization by controlling the equivalent of indanedione and malononitrile from 1:1.4 to 1:1. Isomer-free ITBC shows better performance than isomer mixture ITBTC.[82] However, the dipole moment of regioisomers (TTC EGs) is too small to gain the pure component. This undefined structure sometimes confuses the structure-property relationship.

CF3-IC and its isomer-free EGs are also applied in Y-series.[120] From single-crystal analysis, BTIC-CF_3-γ has a similar single-crystal structure with Y6, which exhibits *J*-aggregation in the horizontal direction between EGs and *H*-aggregation infused core in the perpendicular direction. The 3D interpenetrating framework facilitates charge transport. The PM6: BTIC-CF_3-γ system shows a PCE of 15.59%, comparable with PM6:Y6. Moreover, considering the red-shifted absorption of BTIC-CF_3-γ than Y6, the PM6: BTIC-CF_3-γ: Y6 ternary system achieves a high PCE of 16.5% with a Y6: BTIC-CF_3-γ weight ratio of 10:1.15.

Therefore, it is essential to obtain the isomer-free IC end group to precisely control the composition of the active layer and enhance the device reproductivity. Purifying FREAs and analyzing a single-crystal structure can improve our comprehension of FREAs and provide a guideline to future molecular design.

Interestingly, it has been reported that the efficiency of isomer mixture (COi6-2Cl-*m*) exhibits higher efficiency than that of the isomer-free acceptor (COi6-2Cl-δ and COi6-2Cl-γ).[102] Devices based on isomers (PTB7-Th: COi6-2Cl-*m*) exhibit similar PCE, V_{OC}, J_{SC}, and FF as ternary devices (PTB7-Th: COi6-2Cl-δ and COi6-2Cl-γ). Obtaining isomer-free EGs and establishing clear structure-property relationships in this work is more important than the efficiency.

End-Group Redistribution

Despite the high performance of asymmetric FREAs that has been achieved, the relationship between structure and performance may not be easily ascertained. Gao et al.[58] reported that the redistribution reaction existed in the Knoevenagel condensation reactions, the final step of asymmetric FREAs synthesis. According to the work of the Marks group, this unexpected rearrangement also happens in solution.[60] They prepared solutions in a conventional procedure based on two asymmetric NFAs: IT-2F (IC + 2FIC EGs) and IT-3F (IC + 3FIC EGs) blending with PM6 as the donor, respectively. After stirring at 50°C for 16 h, the IT-2F toluene solution shows F peaks on nuclear magnetic resonance (NMR), which belong to ITIC-0F and ITIC-4F. And the ITIC-2F/ITIC-0F/ITIC-4F ratio is 10:3:3 (60% scrambled). Similar redistribution was found in ITIC-3F, with only 5% scrambled. Moreover, the reverse reaction from two symmetric acceptors (A_1DA_1 and A_2DA_2) to asymmetric acceptors (A_1DA_2) also happens in the blend solution by EG redistribution with CA/CR mechanism (Figure 10). In this case, many binary-blend OPVs based on asymmetric acceptor were actually ternary devices. Likewise, ternary blends with two FREAs are quaternary blends or even more complex if the fused core of FREAs is different. Although the scrambling effect on device performance is not significant in this work, it is not clear in other systems. The end group rearrangement in other systems and how to shift this equilibrium need further investigation.

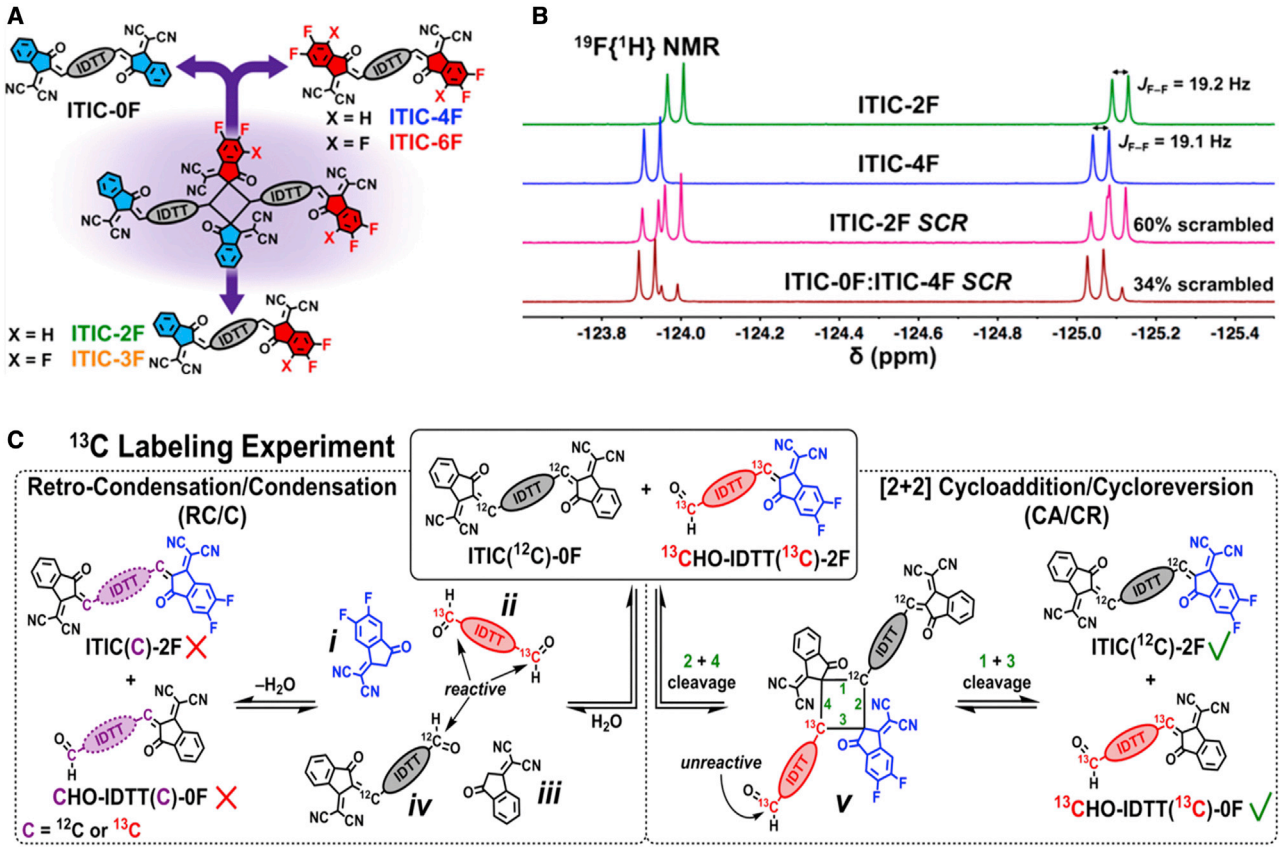

Figure 10. End-Group Redistribution Issue of Asymmetric Substituted FREAs

(A) Redistribution diagram between ITIC-0F: ITIC-4F(ITIC-6F) and ITIC-2F(ITIC-3F).

(B) $^{19}F^{1}H$ NMR spectra of the purified ITIC-2F and ITIC-4F NFAs compared with those of ITIC-2F *SCR* and ITIC-0F:ITIC-4F *SCR* active layer solutions.

(C) (a) Reaction between unlabeled ITIC-0F (1.0 equivalent) and 13CHO-IDTT(13C)-2F (1.0 equivalent) in PhCl:DIO (99.5:0.5 v:v) with PBDB-TF at 50°C for 24 h. Expected products of the RC/C and CA/CR mechanisms are shown. Reprinted with permission from Aldrich et al.[60] Copyright 2019 American Chemical Society.

OPV efficiency breakthroughs bring the dream of industrialization closer. To achieve the goal, we must realize that OPV efficiency, lifetime, materials cost, and manufacturing technology all need to be further addressed. From the angle of molecular design and structure optimization, we view the following directions as in need of the most urgent attention.

Suppressing non-radiative recombination loss: The photo energy loss of state-of-the-art OPVs is about 0.5–0.6 eV higher than crystalline silicon (0.38 eV), perovskite solar cells (0.34 eV), and GaAs (0.32 eV).[180–182] The high energy loss of OPVs is attributed to the CT state and non-radiative loss. Through molecular design, CT state-induced energy loss has been almost eliminated. The non-radiative loss was also significantly reduced, for example, from ITIC series to Y series, which is consistent with the higher electroluminescence quantum efficiency (EQE_{EL}). Furthermore, chlorinated-IC (BTP-4Cl) showed lower energy loss than fluorinated-IC (Y6), suggesting the promising potential of designing new EGs to further reduce energy loss. The molecular design approach can be further combined with a ternary strategy, for example, with deep HOMO third component to reduce V_{OC} energy loss.[183]

Improving material stability: Intrinsic material stability is the cornerstone of device lifetime, which is undoubtedly critical for technology success. The double bonds between fused core and EGs are the most vulnerable. The intrinsic stability of modified IC should be further investigated, such as TC and π-extension IC. Moreover, to solve this problem and maintain the conjugation between fused core and EGs, according to the knowledge of the nonlinear optical materials, nitrogen could be used to replace the carbon atom in double bonds.[184,185] Incorporating non-fullerene small molecular and polymer acceptors has shown evidence of significantly improved OPV light stability, which deserves further exploration.[186]

Simplifying the molecule and reducing the cost: Although OPVs require only a ~100-nm-thick active layer to achieve high efficiency, the coating process prefers thicker film.[187,188] Therefore, the material cost still needs to be on the radar screen. The molecular structures of FREAs have become more complex. For example, according to a previous report, the cost of the FA $PC_{71}BM$ is estimated at about $350 per gram in the current status, $70 per gram in an upscaling model, and $14 per gram in an industrial model. For ITIC-series FREAs, the cost is about $700 per gram in the current status, $150 per gram in an upscaling model, and $35 per gram in an industrial model.[189–191] FREAs have higher cost than FAs. For Y series, more than ten steps are needed to obtain the target acceptor, with the final yield lower than 5% from the raw materials, which is more complex than ITIC.[192] This is acceptable for synthesis in the laboratory but difficult for scaled-up production. This is especially true for the fused core with low-yield annulation reaction and purification, which could impede commercialization. Although high-performance FREAs show less batch-to-batch variation than the polymer donor, designing simple and economical FREAs represents a challenge to conquer in the future.

ACKNOWLEDGMENTS

This work was supported by the Research Grants Council of Hong Kong (project numbers 15218517 and C5037-18G), the National Natural Science Foundation of China (51961165102), the Shenzhen Science and Technology Innovation Commission (JCYJ20170413154602102), and the Hong Kong Polytechnic University Internal Research Funds: Project of Strategic Importance (1-ZE29), Sir Sze-yuen Chung Endowed Professorship Fund (8-8480), University Supporting Fund for Major Research (1-BBAS), and Postdoctoral Fellowships Scheme (YW3Y).

AUTHOR CONTRIBUTIONS

J. H. proposed the review topic and wrote the manuscript. J. H. and H. T. prepared the figures and tables. C. Y. and G. L. supervised the whole project.

DECLARATION OF INTERESTS

The authors declare no competing interests.

REFERENCES

1. Yan, C., Barlow, S., Wang, Z., Yan, H., Jen, A.K.Y., Marder, S.R., and Zhan, X. (2018). Non-fullerene acceptors for organic solar cells. Nat. Rev. Mater. *3*, 18003.

2. Li, G., Chang, W.H., and Yang, Y. (2017). Low-bandgap conjugated polymers enabling solution-processable tandem solar cells. Nat. Rev. Mater. *2*, 17043.

3. Cheng, P., Li, G., Zhan, X., and Yang, Y. (2018). Next-generation organic photovoltaics based on non-fullerene acceptors. Nat. Photonics *12*, 131–142.

4. Zhang, G., Zhao, J., Chow, P.C.Y., Jiang, K., Zhang, J., Zhu, Z., Zhang, J., Huang, F., and Yan, H. (2018). Nonfullerene acceptor molecules for bulk heterojunction organic solar cells. Chem. Rev. *118*, 3447–3507.

5. Chang, S.-Y., Cheng, P., Li, G., and Yang, Y. (2018). Transparent polymer photovoltaics for solar energy harvesting and beyond. Joule *2*, 1039–1054.

6. Bae, S.-H., Zhao, H., Hsieh, Y.-T., Zuo, L., De Marco, N., Rim, Y.S., Li, G., and Yang, Y. (2016). Printable solar cells from advanced solution-processible materials. Chem *1*, 197–219.

7. Li, G., Chu, C.W., Shrotriya, V., Huang, J., and Yang, Y. (2006). Efficient inverted polymer solar cells. Appl. Phys. Lett. *88*, 253503.

8. Yan, C., Ma, R., Cai, G., Liu, T., Zhu, J., Wang, J., Li, Y., Huang, J., Luo, Z., Xiao, Y., et al. (2020). Reducing V_{OC} loss via structure compatible and high lowest unoccupied molecular orbital nonfullerene acceptors for over 17%-efficiency ternary organic photovoltaics. EcoMat. Published online October 26, 2020. https://doi.org/10.1002/eom2.12061.

9. Tang, H., Yan, C., Huang, J., Kan, Z., Xiao, Z., Sun, K., Li, G., and Lu, S. (2020). Benzodithiophene-based small-molecule donors for next-generation all-small-molecule organic photovoltaics. Matter *3*, 1403–1432.

10. Yu, G., Gao, J., Hummelen, J.C., Wudl, F., and Heeger, A.J. (1995). Polymer photovoltaic cells: enhanced efficiencies via a network of internal donor-acceptor heterojunctions. Science *270*, 1789–1791.

11. Benduhn, J., Tvingstedt, K., Piersimoni, F., Ullbrich, S., Fan, Y., Tropiano, M., McGarry, K.A., Zeika, O., Riede, M.K., Douglas, C.J., et al. (2017). Intrinsic non-radiative voltage losses in fullerene-based organic solar cells. Nat. Energy *2*, 17053.

12. Liu, X., Li, Y., Ding, K., and Forrest, S. (2019). Energy loss in organic photovoltaics: nonfullerene versus fullerene acceptors. Phys. Rev. Appl. *11*, 024060.

13. Liu, F., Zhou, Z., Zhang, C., Vergote, T., Fan, H., Liu, F., and Zhu, X. (2016). A thieno[3,4-b] thiophene-based non-fullerene electron acceptor for high-performance bulk-heterojunction organic solar cells. J. Am. Chem. Soc. *138*, 15523–15526.

14. Zhang, G., Yang, G., Yan, H., Kim, J.H., Ade, H., Wu, W., Xu, X., Duan, Y., and Peng, Q. (2017). Efficient nonfullerene polymer solar cells enabled by a novel wide bandgap small molecular acceptor. Adv. Mater. *29*, 1606054.

15. Vartanian, M., Singhal, R., de la Cruz, P., Biswas, S., Sharma, G.D., and Langa, F. (2018). Low energy loss of 0.57 eV and high efficiency of 8.80% in porphyrin-based BHJ solar cells. ACS Appl. Mater. Interfaces *1*, 1304–1315.

16. González, M., Segura, J.L., Seoane, C., Martín, N., Garín, J., Orduna, J., Alcalá, R., Villacampa, B., Hernández, V., and López Navarrete, J.T. (2001). Tetrathiafulvalene derivatives as NLO-phores: synthesis, electrochemistry, Raman spectroscopy, theoretical calculations, and NLO properties of novel TTF-derived donor-π-acceptor dyads. J. Org. Chem. *66*, 8872–8882.

17. Yu, L., Chan, W., Bao, Z., and Cao, S.X.F. (1992). Synthesis and physical measurements of a photorefractive polymer. J. Chem. Soc. Chem. Comm. (23), 1735–1737.

18. Zeigler, D.F., Chen, K.-S., Yip, H.-L., Zhang, Y., and Jen, A.K.-Y. (2012). Tunable light-harvesting polymers containing embedded dipolar chromophores for polymer solar cell applications. J. Polym. Sci. A Polym. Chem. *50*, 1362–1373.

19. Planells, M., and Robertson, N. (2012). Naphthyl derivatives functionalised with electron acceptor units—synthesis, electronic characterisation and DFT calculations. Eur. J. Org. Chem. *2012*, 4947–4953.

20. Yao, C., Yang, Y., Li, L., Bo, M., Zhang, J., Peng, C., Huang, Z., and Wang, J. (2020). Elucidating the key role of the cyano (−CoN) group to construct environmentally friendly fused-ring electron acceptors. J. Phys. Chem. C *124*, 23059–23068.

21. Capobianco, A., Esposito, A., Caruso, T., Borbone, F., Carella, A., Centore, R., and Peluso, A. (2012). Tuning wavefunction mixing in push-pull molecules: from neutral to zwitterionic compounds. Eur. J. Org. Chem. *2012*, 2980–2989.

22. Lin, Y., Wang, J., Zhang, Z.G., Bai, H., Li, Y., Zhu, D., and Zhan, X. (2015). An electron acceptor challenging fullerenes for efficient polymer solar cells. Adv. Mater. *27*, 1170–1174.

23. Liang, Y., Wu, Y., Feng, D., Tsai, S.-T., Son, H.-J., Li, G., and Yu, L. (2009). Development of new semiconducting polymers for high performance solar cells. J. Am. Chem. Soc. *131*, 56–57.

24. Zhao, W., Qian, D., Zhang, S., Li, S., Inganäs, O., Gao, F., and Hou, J. (2016). Fullerene-free polymer solar cells with over 11% efficiency and excellent thermal stability. Adv. Mater. *28*, 4734–4739.

25. Lin, Y., Zhao, F., He, Q., Huo, L., Wu, Y., Parker, T.C., Ma, W., Sun, Y., Wang, C., Zhu, D., et al. (2016). High-performance electron acceptor with thienyl side chains for organic photovoltaics. J. Am. Chem. Soc. *138*, 4955–4961.

26. Dou, L., Gao, J., Richard, E., You, J., Chen, C.C., Cha, K.C., He, Y., Li, G., and Yang, Y. (2012). Systematic investigation of benzodithiophene- and diketopyrrolopyrrole-based low-bandgap polymers designed for single junction and tandem polymer solar cells. J. Am. Chem. Soc. *134*, 10071–10079.

27. Huo, L., Zhang, S., Guo, X., Xu, F., Li, Y., and Hou, J. (2011). Replacing alkoxy groups with alkylthienyl groups: a feasible approach to improve the properties of photovoltaic polymers. Angew. Chem. Int. Ed. Engl. *50*, 9697–9702.

28. Du, X., Heumueller, T., Gruber, W., Classen, A., Unruh, T., Li, N., and Brabec, C.J. (2019). Efficient polymer solar cells based on non-fullerene acceptors with potential device lifetime approaching 10 years. Joule *3*, 215–226.

29. Zhang, Z., Yu, J., Yin, X., Hu, Z., Jiang, Y., Sun, J., Zhou, J., Zhang, F., Russell, T.P., Liu, F., et al. (2018). Conformation locking on fused-ring electron acceptor for high-performance nonfullerene organic solar cells. Adv. Funct. Mater. *28*, 1705095.

30. Kan, B., Feng, H., Wan, X., Liu, F., Ke, X., Wang, Y., Wang, Y., Zhang, H., Li, C., Hou, J., and Chen, Y. (2017). Small-molecule acceptor based on the heptacyclic benzodi(cyclopentadithiophene) unit for highly efficient nonfullerene organic solar cells. J. Am. Chem. Soc. *139*, 4929–4934.

31. Wang, J., Wang, W., Wang, X., Wu, Y., Zhang, Q., Yan, C., Ma, W., You, W., and Zhan, X. (2017). Enhancing performance of nonfullerene acceptors via side-chain conjugation strategy. Adv. Mater. *29*, 1702125.

32. Li, Y., Zhong, L., Gautam, B., Bin, H.-J., Lin, J.-D., Wu, F.-P., Zhang, Z., Jiang, Z.-Q., Zhang, Z.-G., Gundogdu, K., et al. (2017). A near-infrared non-fullerene electron acceptor for high performance polymer solar cells. Energy Environ. Sci. *10*, 1610–1620.

33. Ye, C., Wang, Y., Bi, Z., Guo, X., Fan, Q., Chen, J., Ou, X., Ma, W., and Zhang, M. (2018). High-performance organic solar cells based on a small molecule with thieno[3,2-b]thiophene as π-bridge. Org. Electron. *53*, 273–279.

34. Li, X., Yan, T., Bin, H., Han, G., Xue, L., Liu, F., Yi, Y., Zhang, Z.-G., Russell, T.P., and Li, Y. (2017). Insertion of double bond π-bridges of A–D–A acceptors for high performance near-infrared polymer solar cells. J. Mater. Chem. A Mater. Energy Sustain. *5*, 22588–22597.

35. Lin, Y., Zhang, Z.-G., Bai, H., Wang, J., Yao, Y., Li, Y., Zhu, D., and Zhan, X. (2015). High-performance fullerene-free polymer solar cells with 6.31% efficiency. Energy Environ. Sci. *8*, 610–616.

36. Yao, H., Chen, Y., Qin, Y., Yu, R., Cui, Y., Yang, B., Li, S., Zhang, K., and Hou, J. (2016). Design and synthesis of a low bandgap small molecule acceptor for efficient polymer solar cells. Adv. Mater. *28*, 8283–8287.

37. Liu, Y., Zhang, Z., Feng, S., Li, M., Wu, L., Hou, R., Xu, X., Chen, X., and Bo, Z. (2017). Exploiting noncovalently conformational locking as a design strategy for high performance fused-ring electron acceptor used in polymer solar cells. J. Am. Chem. Soc. *139*, 3356–3359.

38. Zhang, J., Yan, C., Wang, W., Xiao, Y., Lu, X., Barlow, S., Parker, T.C., Zhan, X., and Marder, S.R. (2018). Panchromatic ternary photovoltaic cells using a nonfullerene acceptor synthesized using C–H functionalization. Chem. Mater. *30*, 309–313.

39. Wang, W., Yan, C., Lau, T.K., Wang, J., Liu, K., Fan, Y., Lu, X., and Zhan, X. (2017). Fused hexacyclic nonfullerene acceptor with strong near-infrared absorption for semitransparent organic solar cells with 9.77% efficiency. Adv. Mater. *29*, 1701308.

40. Yuan, J., Huang, T., Cheng, P., Zou, Y., Zhang, H., Yang, J.L., Chang, S.Y., Zhang, Z., Huang, W., Wang, R., et al. (2019). Enabling low voltage losses and high photocurrent in fullerene-free organic photovoltaics. Nat. Commun. *10*, 570.

41. Chen, H. (2019). Electron-deficient core fused-ring based non-Fullerene acceptor enables over 15% efficiency in single junction organic solar cells. Sci. China Chem. *62*, 403–404.

42. Qin, L., Liu, X., Zhang, X., Yu, J., Yang, L., Zhao, F., Huang, M., Wang, K., Wu, X., Li, Y., et al. (2020). Triplet acceptors with a D-A structure and twisted conformation for efficient organic solar cells. Angew. Chem. Int. Ed. Engl. *59*, 2–9.

43. Zhu, L., Zhang, M., Zhou, G., Hao, T., Xu, J., Wang, J., Qiu, C., Prine, N., Ali, J., Feng, W., et al. (2020). Efficient organic solar cell with 16.88% efficiency enabled by refined acceptor

crystallization and morphology with improved charge transfer and transport properties. Adv. Energy Mater. *10*, 1904234.

44. Yuan, J., Zhang, Y., Zhou, L., Zhang, C., Lau, T.K., Zhang, G., Lu, X., Yip, H.L., So, S.K., Beaupré, S., et al. (2019). Fused benzothiadiazole: a building block for n-type organic acceptor to achieve high-performance organic solar cells. Adv. Mater. *31*, e1807577.

45. Zhang, Y., Kan, B., Sun, Y., Wang, Y., Xia, R., Ke, X., Yi, Y.Q., Li, C., Yip, H.L., Wan, X., et al. (2018). Nonfullerene tandem organic solar cells with high performance of 14.11. Adv. Mater. *30*, e1707508.

46. Gao, W., Liu, T., Zhong, C., Zhang, G., Zhang, Y., Ming, R., Zhang, L., Xin, J., Wu, K., Guo, Y., et al. (2018). Asymmetrical small molecule acceptor enabling nonfullerene polymer solar cell with fill factor approaching 79%. ACS Energy Lett. *3*, 1760–1768.

47. Feng, S., Zhang, C., Liu, Y., Bi, Z., Zhang, Z., Xu, X., Ma, W., and Bo, Z. (2017). Fused-ring acceptors with asymmetric side chains for high-performance thick-film organic solar cells. Adv. Mater. *29*, 1703527.

48. Su, W., Fan, Q., Guo, X., Chen, J., Wang, Y., Wang, X., Dai, P., Ye, C., Bao, X., Ma, W., et al. (2018). Significant enhancement of the photovoltaic performance of organic small molecule acceptors via side-chain engineering. J. Mater. Chem. A Mater. Energy Sustain. *6*, 7988–7996.

49. Li, S., Ye, L., Zhao, W., Zhang, S., Mukherjee, S., Ade, H., and Hou, J. (2016). Energy-level modulation of small-molecule electron acceptors to achieve over 12% efficiency in polymer solar cells. Adv. Mater. *28*, 9423–9429.

50. Ye, L., Zhao, W., Li, S., Mukherjee, S., Carpenter, J.H., Awartani, O., Jiao, X., Hou, J., and Ade, H. (2017). High-efficiency nonfullerene organic solar cells: critical factors that affect complex multi-length scale morphology and device performance. Adv. Energy Mater. *7*, 1602000.

51. Xie, S., Xia, Y., Zheng, Z., Zhang, X., Yuan, J., Zhou, H., and Zhang, Y. (2018). Effects of nonradiative losses at charge transfer states and energetic disorder on the open-circuit voltage in nonfullerene organic solar cells. Adv. Funct. Mater. *28*, 1705659.

52. Ke, X., Kan, B., Wan, X., Wang, Y., Zhang, Y., Li, C., and Chen, Y. (2018). Substituents on the end group subtle tuning the energy levels and absorptions of small-molecule nonfullerene acceptors. Dyes Pigm. *155*, 241–248.

53. An, Q., Gao, W., Zhang, F., Wang, J., Zhang, M., Wu, K., Ma, X., Hu, Z., Jiao, C., and Yang, C. (2018). Energy level modulation of non-fullerene acceptors enables efficient organic solar cells with small energy loss. J. Mater. Chem. A Mater. Energy Sustain. *6*, 2468–2475.

54. Lin, Y., Zhao, F., Wu, Y., Chen, K., Xia, Y., Li, G., Prasad, S.K., Zhu, J., Huo, L., Bin, H., et al. (2017). Mapping polymer donors toward high-efficiency fullerene free organic solar cells. Adv. Mater. *29*, 1604155.

55. Lin, Y., Li, T., Zhao, F., Han, L., Wang, Z., Wu, Y., He, Q., Wang, J., Huo, L., Sun, Y., et al. (2016). Structure evolution of oligomer fused-ring electron acceptors toward high efficiency of as-cast polymer solar cells. Adv. Energy Mater. *6*, 1600854.

56. Li, S., Ye, L., Zhao, W., Zhang, S., Ade, H., and Hou, J. (2017). Significant influence of the methoxyl substitution position on optoelectronic properties and molecular packing of small-molecule electron acceptors for photovoltaic cells. Adv. Energy Mater. *7*, 1700183.

57. Zhu, J., Li, S., Liu, X., Yao, H., Wang, F., Zhang, S., Sun, M., and Hou, J. (2017). Subtle side-chain tuning on terminal groups of small molecule electron acceptors for efficient fullerene-free polymer solar cells. J. Mater. Chem. A Mater. Energy Sustain. *5*, 15175–15182.

58. Gao, B., Yao, H., Hou, J., Yu, R., Hong, L., Xu, Y., and Hou, J. (2018). Multi-component non-fullerene acceptors with tunable bandgap structures for efficient organic solar cells. J. Mater. Chem. A Mater. Energy Sustain. *6*, 23644–23649.

59. Li, W., Ye, L., Li, S., Yao, H., Ade, H., and Hou, J. (2018). A high-efficiency organic solar cell enabled by the strong intramolecular electron push-pull effect of the nonfullerene acceptor. Adv. Mater. *30*, e1707170.

60. Aldrich, T.J., Matta, M., Zhu, W., Swick, S.M., Stern, C.L., Schatz, G.C., Facchetti, A., Melkonyan, F.S., and Marks, T.J. (2019). Fluorination effects on indacenodithienothiophene acceptor packing and electronic structure, end-group redistribution, and solar cell photovoltaic response. J. Am. Chem. Soc. *141*, 3274–3287.

61. Dai, S., Zhao, F., Zhang, Q., Lau, T.K., Li, T., Liu, K., Ling, Q., Wang, C., Lu, X., You, W., and Zhan, X. (2017). Fused nonacyclic electron acceptors for efficient polymer solar cells. J. Am. Chem. Soc. *139*, 1336–1343.

62. Li, Z., Dai, S., Xin, J., Zhang, L., Wu, Y., Rech, J., Zhao, F., Li, T., Liu, K., Liu, Q., et al. (2018). Enhancing the performance of the electron acceptor ITIC-Th via tailoring its end groups. Mater. Chem. Front. *2*, 537–543.

63. Fan, Q., Su, W., Zhang, M., Wu, J., Jiang, Y., Guo, X., Liu, F., Russell, T.P., Zhang, M., and Li, Y. (2019). Synergistic effects of side-chain engineering and fluorination on small molecule acceptors to simultaneously broaden spectral response and minimize voltage loss for 13.8% efficiency organic solar cells. Solar RRL *3*, 1900169.

64. Li, X., Yao, J., Angunawela, I., Sun, C., Xue, L., Liebman-Pelaez, A., Zhu, C., Yang, C., Zhang, Z.-G., Ade, H., et al. (2018). Improvement of photovoltaic performance of polymer solar cells by rational molecular optimization of organic molecule acceptors. Adv. Energy Mater. *8*, 1800815.

65. Zhang, H., Yao, H., Hou, J., Zhu, J., Zhang, J., Li, W., Yu, R., Gao, B., Zhang, S., and Hou, J. (2018). Over 14% efficiency in organic solar cells enabled by chlorinated nonfullerene small-molecule acceptors. Adv. Mater. *30*, e1800613.

66. Wan, S.S., Chang, C., Wang, J.L., Yuan, G.Z., Wu, Q., Zhang, M., and Li, Y. (2018). Effects of the number of bromine substitution on photovoltaic efficiency and energy loss of benzo[1,2-b:4,5-b¢]diselenophene-based narrow-bandgap multibrominated nonfullerene acceptors. Solar RRL *3*, 1800250.

67. Li, Y., Lin, J.D., Che, X., Qu, Y., Liu, F., Liao, L.S., and Forrest, S.R. (2017). High efficiency near-infrared and semitransparent non-fullerene acceptor organic photovoltaic cells. J. Am. Chem. Soc. *139*, 17114–17119.

68. Chen, Y., Liu, T., Hu, H., Ma, T., Lai, J.Y.L., Zhang, J., Ade, H., and Yan, H. (2018). Modulation of end groups for low-bandgap nonfullerene acceptors enabling high-performance organic solar cells. Adv. Energy Mater. *8*, 1801203.

69. Yao, H., Cui, Y., Yu, R., Gao, B., Zhang, H., and Hou, J. (2017). Design, synthesis, and photovoltaic characterization of a small molecular acceptor with an ultra-narrow band gap. Angew. Chem. Int. Ed. Engl. *56*, 3045–3049.

70. Yao, H., Ye, L., Hou, J., Jang, B., Han, G., Cui, Y., Su, G.M., Wang, C., Gao, B., Yu, R., et al. (2017). Achieving highly efficient nonfullerene organic solar cells with improved intermolecular interaction and open-circuit voltage. Adv. Mater. *29*, 1700254.

71. Sun, J., Zhang, Z., Yin, X., Zhou, J., Yang, L., Geng, R., Zhang, F., Zhu, R., Yu, J., and Tang, W. (2018). High performance non-fullerene polymer solar cells based on PTB7-Th as the electron donor with 10.42% efficiency. J. Mater. Chem. A Mater. Energy Sustain. *6*, 2549–2554.

72. Xie, D., Liu, T., Gao, W., Zhong, C., Huo, L., Luo, Z., Wu, K., Xiong, W., Liu, F., Sun, Y., et al. (2017). A novel thiophene-fused ending group enabling an excellent small molecule acceptor for high-performance fullerene-free polymer solar cells with 11.8% efficiency. Solar RRL *1*, 1700044.

73. Cui, Y., Yao, H., Gao, B., Qin, Y., Zhang, S., Yang, B., He, C., Xu, B., and Hou, J. (2017). Fine-tuned photoactive and interconnection layers for achieving over 13% efficiency in a fullerene-free tandem organic solar cell. J. Am. Chem. Soc. *139*, 7302–7309.

74. Luo, Z., Bin, H., Liu, T., Zhang, Z.G., Yang, Y., Zhong, C., Qiu, B., Li, G., Gao, W., Xie, D., et al. (2018). Fine-tuning of molecular packing and energy level through methyl substitution enabling excellent small molecule acceptors for nonfullerene polymer solar cells with efficiency up to 12.54. Adv. Mater. *30*, 1706124.

75. Yan, D., Liu, W., Yao, J., and Zhan, C. (2018). Fused-ring nonfullerene acceptor forming interpenetrating j-architecture for fullerene-free polymer solar cells. Adv. Energy Mater. *8*, 1800204.

76. Zhang, J., Li, Y., Hu, H., Zhang, G., Ade, H., and Yan, H. (2019). Chlorinated thiophene end groups for highly crystalline alkylated non-fullerene acceptors toward efficient organic solar cells. Chem. Mater. *31*, 6672–6676.

77. Ni, S.-S., Xu, X., Wang, J.-L., Wan, S.-S., Liu, K.-K., Bai, H.-R., Yang, C., Lv, G., and Peng, Q. (2019). Regioisomer-free chlorinated

thiophene-based ending group for thieno [3,2-b]thiophene central unit-based acceptor enabling highly efficient nonfullerene polymer solar cells with high V_{oc} simultaneously. Solar RRL *4*, 1900446.

78. Luo, Z., Liu, T., Wang, Y., Zhang, G., Sun, R., Chen, Z., Zhong, C., Wu, J., Chen, Y., Zhang, M., et al. (2019). Reduced energy loss enabled by a chlorinated thiophene-fused ending-group small molecular acceptor for efficient nonfullerene organic solar cells with 13.6% efficiency. Adv. Energy Mater. *9*, 1900041.

79. Luo, Z., Liu, T., Xiao, Y., Yang, T., Chen, Z., Zhang, G., Zhong, C., Ma, R., Chen, Y., Zou, Y., et al. (2019). Significantly improving the performance of polymer solar cells by the isomeric ending-group based small molecular acceptors: insight into the isomerization. Nano Energy *66*, 104146.

80. Li, S., Ye, L., Zhao, W., Liu, X., Zhu, J., Ade, H., and Hou, J. (2017). Design of a new small-molecule electron acceptor enables efficient polymer solar cells with high fill factor. Adv. Mater. *29*, 1704051.

81. Swick, S.M., Zhu, W., Matta, M., Aldrich, T.J., Harbuzaru, A., Lopez Navarrete, J.T., Ponce Ortiz, R., Kohlstedt, K.L., Schatz, G.C., Facchetti, A., et al. (2018). Closely packed, low reorganization energy π-extended postfullerene acceptors for efficient polymer solar cells. Proc. Natl. Acad. Sci. U S A *115*, E8341–E8348.

82. Yang, K., Liao, Q., Koh, C.W., Chen, J., Su, M., Zhou, X., Tang, Y., Wang, Y., Zhang, Y., Woo, H.Y., et al. (2019). Improved photovoltaic performance of a nonfullerene acceptor based on a benzo[b]thiophene fused end group with extended π-conjugation. J. Mater. Chem. A Mater. Energy Sustain. *7*, 9822–9830.

83. Chang, S.L., Hung, K.E., Cao, F.Y., Huang, K.H., Hsu, C.S., Liao, C.Y., Lee, C.H., and Cheng, Y.J. (2019). Isomerically pure benzothiophene-incorporated acceptor: achieving improved V_{oc} and J_{sc} of nonfullerene organic solar cells via end group manipulation. ACS Appl. Mater. Interfaces *11*, 33179–33187.

84. Chang, S.-L., Cao, F.-Y., Huang, W.-C., Huang, P.-K., Huang, K.-H., Hsu, C.-S., and Cheng, Y.-J. (2018). New thieno[3,2-b] thiophene-based acceptor: tuning acceptor strength of ladder-type N-type materials to simultaneously achieve enhanced V_{oc} and J_{sc} of nonfullerene solar cells. ACS Energy Lett. *3*, 1722–1729.

85. Swick, S.M., Alzola, J.M., Sangwan, V.K., Amsterdam, S.H., Zhu, W., Jones, L.O., Powers-Riggs, N., Facchetti, A., Kohlstedt, K.L., Schatz, G.C., et al. (2020). Fluorinating π-extended molecular acceptors yields highly connected crystal structures and low reorganization energies for efficient solar cells. Adv. Energy Mater. *10*, 2000635.

86. Wan, S.-S., Xu, X., Jiang, Z., Yuan, J., Mahmood, A., Yuan, G.-Z., Liu, K.-K., Ma, W., Peng, Q., and Wang, J.-L. (2020). A bromine and chlorine concurrently functionalized end group for benzo[1,2-b:4,5-b¢]diselenophene-based non-fluorinated acceptors: a new hybrid strategy to balance the crystallinity and miscibility of blend films for enabling highly efficient polymer solar cells. J. Mater. Chem. A Mater. Energy Sustain. *8*, 4856–4867.

87. Hao, M., Liu, T., Xiao, Y., Ma, L.-K., Zhang, G., Zhong, C., Chen, Z., Luo, Z., Lu, X., Yan, H., et al. (2019). Achieving balanced charge transport and favorable blend morphology in non-fullerene solar cells via acceptor end group modification. Chem. Mater. *31*, 1752–1760.

88. Feng, S., Ma, D., Wu, L., Liu, Y., Zhang, C.e., Xu, X., Chen, X., Yan, S., and Bo, Z. (2018). Enhance the performance of polymer solar cells via extension of the flanking end groups of fused ring acceptors. Sci. China Chem. *61*, 1320–1327.

89. Li, S., Zhan, L., Sun, C., Zhu, H., Zhou, G., Yang, W., Shi, M., Li, C.Z., Hou, J., Li, Y., and Chen, H. (2019). Highly efficient fullerene-free organic solar cells operate at near zero highest occupied molecular orbital offsets. J. Am. Chem. Soc. *141*, 3073–3082.

90. Yu, R., Yao, H., Hong, L., Xu, Y., Gao, B., Zhu, J., Zu, Y., and Hou, J. (2018). Enhancing the photovoltaic performance of nonfullerene acceptors via conjugated rotatable end groups. Adv. Energy Mater. *8*, 1802131.

91. Li, R., Liu, G., Xie, R., Wang, Z., Yang, X., An, K., Zhong, W., Jiang, X.-F., Ying, L., Huang, F., et al. (2018). Introducing cyclic alkyl chains into small-molecule acceptors for efficient polymer solar cells. J. Mater. Chem. C Mater. Opt. Electron. Devices *6*, 7046–7053.

92. Liu, X., Wang, X., Xiao, Y., Yang, Q., Guo, X., and Li, C. (2020). H-bonds-assisted molecular order manipulation of nonfullerene acceptors for efficient nonannealed organic solar cells. Adv. Energy Mater. *10*, 1903650.

93. Yao, C., Zhao, J., Zhu, Y., Liu, B., Yan, C., Perepichka, D.F., and Meng, H. (2020). Trifluoromethyl group-modified non-fullerene acceptor toward improved power conversion efficiency over 13% in polymer solar cells. ACS Appl. Mater. Interfaces *12*, 11543–11550.

94. Deng, M., Xu, X., Yu, L., Li, R., and Peng, Q. (2020). Fused ring non-fullerene acceptors with benzothiophene dioxide end groups and their side chain effect investigations. Dyes Pigm. *180*, 108452.

95. Cui, Y., Wang, Y., Bergqvist, J., Yao, H., Xu, Y., Gao, B., Yang, C., Zhang, S., Inganäs, O., Gao, F., et al. (2019). Wide-gap non-fullerene acceptor enabling high-performance organic photovoltaic cells for indoor applications. Nat. Energy *4*, 768–775.

96. Li, M., Zhou, Y., Zhang, J., Song, J., and Bo, Z. (2019). Tuning the dipole moments of nonfullerene acceptors with an asymmetric terminal strategy for highly efficient organic solar cells. J. Mater. Chem. A Mater. Energy Sustain. *7*, 8889–8896.

97. Lai, H., Chen, H., Zhou, J., Qu, J., Wang, M., Xie, W., Xie, Z., and He, F. (2019). 3D interpenetrating network for high-performance nonfullerene acceptors via asymmetric chlorine substitution. J. Phys. Chem. Lett. *10*, 4737–4743.

98. Sun, H., Liu, T., Yu, J., Lau, T.-K., Zhang, G., Zhang, Y., Su, M., Tang, Y., Ma, R., Liu, B., et al. (2019). A monothiophene unit incorporating both fluoro and ester substitution enabling high-performance donor polymers for non-fullerene solar cells with 16.4% efficiency. Energy Environ. Sci. *12*, 3328–3337.

99. Lai, H., Chen, H., Shen, Y., Wang, M., Chao, P., Xie, W., Qu, J., Yang, B., and He, F. (2019). Using chlorine atoms to fine-tune the intermolecular packing and energy levels of efficient nonfullerene acceptors. ACS Appl. Energy Mater. *2*, 7663–7669.

100. Lai, H., Chen, H., Zhou, J., Qu, J., Chao, P., Liu, T., Chang, X., Zheng, N., Xie, Z., and He, F. (2019). Isomer-free: precise positioning of chlorine-induced interpenetrating charge transfer for elevated solar conversion. iScience *17*, 302–314.

101. Qu, J., Li, D., Wang, H., Zhou, J., Zheng, N., Lai, H., Liu, T., Xie, Z., and He, F. (2019). Bromination of the small-molecule acceptor with fixed position for high-performance solar cells. Chem. Mater. *31*, 8044–8051.

102. Liu, T., Zhao, Q., Wang, H., Qu, J., Chao, P., Zheng, N., Lai, H., Mo, D., and He, F. (2019). Carbon–oxygen-bridged hexacyclic non-fullerene acceptors with chlorinated end groups. Mater. Chem. Front. *3*, 1859–1865.

103. Lai, H., Chen, H., Zhu, Y., Chen, L., Huang, H.-H., and He, F. (2020). An asymmetrical A–DAD–A-type acceptor simultaneously enhances voltage and current for efficient organic solar cells. J. Mater. Chem. A Mater. Energy Sustain. *8*, 9670–9676.

104. Zhan, L., Li, S., Lau, T.-K., Cui, Y., Lu, X., Shi, M., Li, C.-Z., Li, H., Hou, J., and Chen, H. (2020). Over 17% efficiency ternary organic solar cells enabled by two non-fullerene acceptors working in an alloy-like model. Energy Environ. Sci. *13*, 635–645.

105. Yuan, J., Zhang, Y., Zhou, L., Zhang, G., Yip, H.-L., Lau, T.-K., Lu, X., Zhu, C., Peng, H., Johnson, P.A., et al. (2019). Single-junction organic solar cell with over 15% efficiency using fused-ring acceptor with electron-deficient core. Joule *3*, 1140–1151.

106. Wang, R., Yuan, J., Wang, R., Han, G., Huang, T., Huang, W., Xue, J., Wang, H.C., Zhang, C., Zhu, C., et al. (2019). Rational tuning of molecular interaction and energy level alignment enables high-performance organic photovoltaics. Adv. Mater. *31*, e1904215.

107. Luo, M., Zhou, L., Yuan, J., Zhu, C., Cai, F., Hai, J., and Zou, Y. (2020). A new non-fullerene acceptor based on the heptacyclic benzotriazole unit for efficient organic solar cells. J. Energy Chem. *42*, 169–173.

108. Luo, M., Zhao, C., Yuan, J., Hai, J., Cai, F., Hu, Y., Peng, H., Bai, Y., Tan, Z.a., and Zou, Y. (2019). Semitransparent solar cells with over 12% efficiency based on a new low bandgap fluorinated small molecule acceptor. Mater. Chem. Front. *3*, 2483–2490.

109. Xu, Y., Yao, H., Ma, L., Hong, L., Li, J., Liao, Q., Zu, Y., Wang, J., Gao, M., Ye, L., and Hou, J. (2020). Tuning the hybridization of local exciton and charge-transfer states in highly efficient organic photovoltaic cells. Angew. Chem. Int. Ed. Engl. *59*, 9004–9010.

110. Luo, M., Zhu, C., Yuan, J., Zhou, L., Keshtov, M.L., Godovsky, D.Y., and Zou, Y. (2019). A chlorinated non-fullerene acceptor for

efficient polymer solar cells. Chin. Chem. Lett. *30*, 2343–2346.

111. Cui, Y., Yao, H., Zhang, J., Zhang, T., Wang, Y., Hong, L., Xian, K., Xu, B., Zhang, S., Peng, J., et al. (2019). Over 16% efficiency organic photovoltaic cells enabled by a chlorinated acceptor with increased open-circuit voltages. Nat. Commun. *10*, 2515.

112. Cui, Y., Yao, H., Hong, L., Zhang, T., Tang, Y., Lin, B., Xian, K., Gao, B., An, C., Bi, P., et al. (2020). Organic photovoltaic cell with 17% efficiency and superior processability. Natl. Sci. Rev. *7*, 1239–1246.

113. Yu, H., Ma, R., Xiao, q., Zhang, J., Liu, T., Luo, Z., Chen, Y., Bai, F., Lu, X., Yan, H., et al. (2020). Improved organic solar cell efficiency based on regulation of alkyl chain on chlorinated non-fullerene acceptors. Mater. Chem. Front. *4*, 2428–2434.

114. Hong, L., Yao, H., Wu, Z., Cui, Y., Zhang, T., Xu, Y., Yu, R., Liao, Q., Gao, B., Xian, K., et al. (2019). Eco-compatible solvent-processed organic photovoltaic cells with over 16% efficiency. Adv. Mater. *31*, e1903441.

115. Jiang, K., Wei, Q., Lai, J.Y.L., Peng, Z., Kim, H.K., Yuan, J., Ye, L., Ade, H., Zou, Y., and Yan, H. (2019). Alkyl chain tuning of small molecule acceptors for efficient organic solar cells. Joule *3*, 3020–3033.

116. Xu, X.P., Feng, K., Lee, Y.W., Woo, H.Y., Zhang, G.J., and Peng, Q. (2020). Subtle polymer donor and molecular acceptor design enable efficient polymer solar cells with a very small energy loss. Adv. Funct. Mater. *30*, 1907570.

117. Li, X., Pan, M.-A., Lau, T.-K., Liu, W., Li, K., Yao, N., Shen, F., Huo, S., Zhang, F., Wu, Y., et al. (2020). Roles of acceptor guests in tuning the organic solar cell property based on an efficient binary material system with a nearly zero hole-transfer driving force. Chem. Mater. *32*, 5182–5191.

118. Qin, R., Wang, D., Zhou, G., Yu, Z.-P., Li, S., Li, Y., Liu, Z.-X., Zhu, H., Shi, M., Lu, X., et al. (2019). Tuning terminal aromatics of electron acceptors to achieve high-efficiency organic solar cells. J. Mater. Chem. A Mater. Energy Sustain. *7*, 27632–27639.

119. Luo, Z., Ma, R., Chen, Z., Xiao, Y., Zhang, G., Liu, T., Sun, R., Zhan, Q., Zou, Y., Zhong, C., et al. (2020). Altering the positions of chlorine and bromine substitution on the end group enables high-performance acceptor and efficient organic solar cells. Adv. Energy Mater. *10*, 2002649.

120. Lai, H., Zhao, Q., Chen, Z., Chen, H., Chao, P., Zhu, Y., Lang, Y., Zhen, N., Mo, D., Zhang, Y., et al. (2020). Trifluoromethylation enables a 3D interpenetrated low-band-gap acceptor for efficient organic solar cells. Joule *4*, 688–700.

121. Yang, C., Zhang, S., Ren, J., Gao, M., Bi, P., Ye, L., and Hou, J. (2020). Molecular design of a non-fullerene acceptor enables a P3HT-based organic solar cell with 9.46% efficiency. Energy Environ. Sci. *13*, 2864–2869.

122. Tao, L., Liu, X., Deng, C., Zhang, W., and Song, W. (2020). Highly efficient nonfullerene acceptor with sulfonyl-based ending groups. ACS Appl. Mater. Interfaces *12*, 49659–49665.

123. Li, S., Zhan, L., Jin, Y., Zhou, G., Lau, T.K., Qin, R., Shi, M., Li, C.Z., Zhu, H., Lu, X., et al. (2020). Asymmetric electron acceptors for high-efficiency and low-energy-loss organic photovoltaics. Adv. Mater. *32*, e2001160.

124. Liu, T., Zhang, Y., Shao, Y., Ma, R., Luo, Z., Xiao, Y., Yang, T., Lu, X., Yuan, Z., Yan, H., et al. (2020). Asymmetric acceptors with fluorine and chlorine substitution for organic solar cells toward 16.83% efficiency. Adv. Funct. Mater. *30*, 2000456.

125. Luo, Z., Ma, R., Liu, T., Yu, J., Xiao, Y., Sun, R., Xie, G., Yuan, J., Chen, Y., Chen, K., et al. (2020). Fine-tuning energy levels via asymmetric end groups enables polymer solar cells with efficiencies over 17%. Joule *4*, 1236–1247.

126. Chen, H., Lai, H., Chen, Z., Zhu, Y., Wang, H., Han, L., Zhang, Y., and He, F. (2020). 17.1%-efficient eco-compatible organic solar cells from a dissymmetric 3D network acceptor. Angew. Chem. Int. Ed. Engl. Published online October 23, 2020. https://doi.org/10.1002/anie.202013053.

127. Wang, T., and Brédas, J.-L. (2020). Organic solar cells based on non-fullerene small-molecule acceptors: impact of substituent position. Matter *2*, 119–135.

128. Bi, Z., and Ma, W. (2020). Calculating structure-performance relationship in organic solar cells. Matter *2*, 14–16.

129. Wang, T., and Brédas, J.-L. (2019). Nonfullerene small-molecule acceptors for organic photovoltaics: understanding the impact of methoxy substitution position on molecular packing and electron-transfer properties. Adv. Funct. Mater. *29*, 1806845.

130. Zhao, W., Li, S., Yao, H., Zhang, S., Zhang, Y., Yang, B., and Hou, J. (2017). Molecular optimization enables over 13% efficiency in organic solar cells. J. Am. Chem. Soc. *139*, 7148–7151.

131. Li, J., Zhang, Y., Yuan, J., Zhu, C., Peng, H., and Zou, Y. (2020). Fine-tuning of non-fullerene acceptor gives over 14% efficiency for organic solar cells. Dyes Pigments *181*, 108559.

132. Liu, S., Yuan, J., Deng, W., Luo, M., Xie, Y., Liang, Q., Zou, Y., He, Z., Wu, H., and Cao, Y. (2020). High-efficiency organic solar cells with low non-radiative recombination loss and low energetic disorder. Nat. Photonics *14*, 300.

133. Cui, Y., Yang, C., Yao, H., Zhu, J., Wang, Y., Jia, G., Gao, F., and Hou, J. (2017). Efficient semitransparent organic solar cells with tunable color enabled by an ultralow-bandgap nonfullerene acceptor. Adv. Mater. *29*, 1703080.

134. Yan, C., Yang, T., Gao, W., Xiao, Y., Li, Y., Lu, X., Yang, C., and Li, G. (2019). Chlorination strategy-induced abnormal nanomorphology tuning in high-efficiency organic solar cells: a study of phenyl-substituted benzodithiophene-based nonfullerene acceptors. Solar RRL *3*, 1900262.

135. Liu, G., Jia, T., Zhang, K., Jia, J., Yin, Q., Zhong, W., Jia, X.e., Zheng, N., Ying, L., Huang, F., et al. (2020). Chlorinated fused nonacyclic non-fullerene acceptor enables efficient large-area polymer solar cells with high scalability. Chem. Mater. *32*, 1022–1030.

136. Yang, F., Li, C., Lai, W., Zhang, A., Huang, H., and Li, W. (2017). Halogenated conjugated molecules for ambipolar field-effect transistors and non-fullerene organic solar cells. Mater. Chem. Front. *1*, 1389–1395.

137. Wang, Y., Zhang, Y., Qiu, N., Feng, H., Gao, H., Kan, B., Ma, Y., Li, C., Wan, X., and Chen, Y. (2018). A halogenation strategy for over 12% efficiency nonfullerene organic solar cells. Adv. Energy Mater. *8*, 1702870.

138. Lu, S., Li, F., Zhang, K., Zhu, J., Cui, W., Yang, R., Yu, L., and Sun, M. (2020). Halogenation on terminal groups of ITIC based electron acceptors as an effective strategy for efficient polymer solar cells. Sol. Energy *195*, 429–435.

139. Guo, B., Li, W., Luo, G., Guo, X., Yao, H., Zhang, M., Hou, J., Li, Y., and Wong, W.-Y. (2018). Exceeding 14% efficiency for solution-processed tandem organic solar cells combining fullerene- and nonfullerene-based subcells with complementary absorption. ACS Energy Lett. *3*, 2566–2572.

140. Liu, G., Jia, J., Zhang, K., Jia, X.e., Yin, Q., Zhong, W., Li, L., Huang, F., and Cao, Y. (2019). 15% efficiency tandem organic solar cell based on a novel highly efficient wide-bandgap nonfullerene acceptor with low energy loss. Adv. Energy Mater. *9*, 1803657.

141. Ho, C.H.Y., Kim, T., Xiong, Y., Firdaus, Y., Yi, X., Dong, Q., Rech, J.J., Gadisa, A., Booth, R., O'Connor, B.T., et al. (2020). High-performance tandem organic solar cells using hsolar as the interconnecting layer. Adv. Energy Mater. *10*, 2000823.

142. Liu, C., Du, X., Gao, S., Classen, A., Osvet, A., He, Y., Mayrhofer, K., Li, N., and Brabec, C.J. (2020). A cross-linked interconnecting layer enabling reliable and reproducible solution-processing of organic tandem solar cells. Adv. Energy Mater. *10*, 1903800.

143. Yan, C., Wang, W., Lau, T.-K., Li, K., Wang, J., Liu, K., Lu, X., and Zhan, X. (2018). Enhancing the performance of non-fullerene organic solar cells via end group engineering of fused-ring electron acceptors. J. Mater. Chem. A Mater. Energy Sustain. *6*, 16638–16644.

144. Luo, Z., Zhao, Y., Zhang, Z.G., Li, G., Wu, K., Xie, D., Gao, W., Li, Y., and Yang, C. (2017). Side-chain effects on energy-level modulation and device performance of organic semiconductor acceptors in organic solar cells. ACS Appl. Mater. Interfaces *9*, 34146–34152.

145. Luo, Z., Sun, C., Chen, S., Zhang, Z.-G., Wu, K., Qiu, B., Yang, C., Li, Y., and Yang, C. (2018). Side-chain impact on molecular orientation of organic semiconductor acceptors: high performance nonfullerene polymer solar cells with thick active layer over 400 nm. Adv. Energy Mater. *8*, 1800856.

146. Liu, K.-K., Xu, X., Wang, J.-L., Zhang, C., Ge, G.-Y., Zhuang, F.-D., Zhang, H.-J., Yang, C., Peng, Q., and Pei, J. (2019). Achieving high-performance non-halogenated nonfullerene acceptor-based organic solar cells with 13.7% efficiency via a synergistic strategy of an indacenodithieno[3,2-b]selenophene core

unit and non-halogenated thiophene-based terminal group. J. Mater. Chem. A Mater. Energy Sustain. *7*, 24389–24399.

147. Zhang, Z., Feng, L., Xu, S., Yuan, J., Zhang, Z.-G., Peng, H., Li, Y., and Zou, Y. (2017). Achieving over 10% efficiency in a new acceptor ITTC and its blends with hexafluoroquinoxaline based polymers. J. Mater. Chem. A Mater. Energy Sustain. *5*, 11286–11293.

148. Gao, W., Liu, T., Ming, R., Luo, Z., Wu, K., Zhang, L., Xin, J., Xie, D., Zhang, G., Ma, W., et al. (2018). Near-infrared small molecule acceptor enabled high-performance nonfullerene polymer solar cells with over 13% efficiency. Adv. Funct. Mater. *28*, 1803128.

149. Liu, W., Li, W., Yao, J., and Zhan, C. (2018). Achieving high short-circuit current and fill-factor via increasing quinoidal character on nonfullerene small molecule acceptor. Chin. Chem. Lett. *29*, 381–384.

150. Gao, W., An, Q., Zhong, C., Luo, Z., Ming, R., Zhang, M., Zou, Y., Liu, F., Zhang, F., and Yang, C. (2018). Designing an asymmetrical isomer to promote the LUMO energy level and molecular packing of a non-fullerene acceptor for polymer solar cells with 12.6% efficiency. Chem. Sci. (Camb.) *9*, 8142–8149.

151. Zhang, Y., Cai, F., Yuan, J., Wei, Q., Zhou, L., Qiu, B., Hu, Y., Li, Y., Peng, H., and Zou, Y. (2019). A new non-fullerene acceptor based on the combination of a heptacyclic benzothiadiazole unit and a thiophene-fused end group achieving over 13% efficiency. Phys. Chem. Chem. Phys. *21*, 26557–26563.

152. Feng, H., Qiu, N., Wang, X., Wang, Y., Kan, B., Wan, X., Zhang, M., Xia, A., Li, C., Liu, F., et al. (2017). An A-D-A type small-molecule electron acceptor with end-extended conjugation for high performance organic solar cells. Chem. Mater. *29*, 7908–7917.

153. Wang, X., Han, J., Jiang, H., Liu, Z., Li, Y., Yang, C., Yu, D., Bao, X., and Yang, R. (2019). Regulation of molecular packing and blend morphology by finely tuning molecular conformation for high-performance nonfullerene polymer solar cells. ACS Appl. Mater. Interfaces *11*, 44501–44512.

154. Feng, H., Yi, Y.-Q.-Q., Ke, X., Zhang, Y., Wan, X., Li, C., and Chen, Y. (2018). Synergistic modifications of side chains and end groups in small molecular acceptors for high efficient non-fullerene organic solar cells. Solar RRL *2*, 1800053.

155. Swick, S.M., Gebraad, T., Jones, L., Fu, B., Aldrich, T.J., Kohlstedt, K.L., Schatz, G.C., Facchetti, A., and Marks, T.J. (2019). Building blocks for high-efficiency organic photovoltaics: interplay of molecular, crystal, and electronic properties in post-fullerene ITIC ensembles. ChemPhysChem *20*, 2608–2626.

156. Chang, M., Wang, Y., Yi, Y.-Q.-Q., Ke, X., Wan, X., Li, C., and Chen, Y. (2018). Fine-tuning the side-chains of non-fullerene small molecule acceptors to match with appropriate polymer donors. J. Mater. Chem. A Mater. Energy Sustain. *6*, 8586–8594.

157. Gao, W., An, Q., Hao, M., Sun, R., Yuan, J., Zhang, F., Ma, W., Min, J., and Yang, C. (2020). Thick-film organic solar cells achieving over 11% efficiency and nearly 70% fill factor at thickness over 400 nm. Adv. Funct. Mater. *30*, 1908336.

158. Wang, Y., Fan, Q., Guo, X., Li, W., Guo, B., Su, W., Ou, X., and Zhang, M. (2017). High-performance nonfullerene polymer solar cells based on a fluorinated wide bandgap copolymer with a high open-circuit voltage of 1.04 V. J. Mater. Chem. A Mater. Energy Sustain. *5*, 22180–22185.

159. Ye, L., Xie, Y., Xiao, Y., Song, J., Li, C., Fu, H., Weng, K., Lu, X., Tan, S., and Sun, Y. (2019). Asymmetric fused-ring electron acceptor with two distinct terminal groups for efficient organic solar cells. J. Mater. Chem. A Mater. Energy Sustain. *7*, 8055–8060.

160. Perdigón-Toro, L., Zhang, H., Markina, A., Yuan, J., Hosseini, S.M., Wolff, C.M., Zuo, G., Stolterfoht, M., Zou, Y., Gao, F., et al. (2020). Barrierless free charge generation in the high-performance pm6:y6 bulk heterojunction non-fullerene solar cell. Adv. Mater. *32*, e1906763.

161. Sun, H., Chen, F., and Chen, Z.-K. (2019). Recent progress on non-fullerene acceptors for organic photovoltaics. Mater. Today *24*, 94–118.

162. Wu, L., Huang, J., Xie, Y., Hong, L., Peng, R., Song, W., Huang, L., Zhu, L., Bi, W., and Ge, Z. (2019). Significant efficiency improvement enabled by CdSe/ZnS quantum dot modifier in organic solar cells. Solar RRL *3*, 1900117.

163. Xu, Y., Yao, H., and Hou, J. (2019). Recent advances in fullerene-free polymer solar cells: materials and devices. Chin. J. Chem. *37*, 207–215.

164. Naveed, H.B., and Ma, W. (2018). Miscibility-driven optimization of nanostructures in ternary organic solar cells using non-fullerene acceptors. Joule *2*, 621–641.

165. Firdaus, Y., Le Corre, V.M., Karuthedath, S., Liu, W., Markina, A., Huang, W., Chattopadhyay, S., Nahid, M.M., Nugraha, M.I., Lin, Y., et al. (2020). Long-range exciton diffusion in molecular non-fullerene acceptors. Nat. Commun. *11*, 5220.

166. Sun, R., Wu, Q., Guo, J., Wang, T., Wu, Y., Qiu, B., Luo, Z., Yang, W., Hu, Z., Guo, J., et al. (2020). A layer-by-layer architecture for printable organic solar cells overcoming the scaling lag of module efficiency. Joule *4*, 407–419.

167. Sun, R., Guo, J., Sun, C., Wang, T., Luo, Z., Zhang, Z., Jiao, X., Tang, W., Yang, C., Li, Y., et al. (2019). A universal layer-by-layer solution-processing approach for efficient non-fullerene organic solar cells. Energy Environ. Sci. *12*, 384–395.

168. Ma, L., Zhang, S., Yao, H., Xu, Y., Wang, J., Zu, Y., and Hou, J. (2020). High-efficiency nonfullerene organic solar cells enabled by 1000 nm thick active layers with a low trap-state density. ACS Appl. Mater. Interfaces *12*, 18777–18784.

169. Lee, D.H., Michael Yang, Y., You, J., Richard, E., and Li, G. (2014). Immiscible solvents enabled nanostructure formation for efficient polymer photovoltaic cells. Nanotechnology *25*, 295401.

170. Liu, Y., Liu, F., Wang, H.W., Nordlund, D., Sun, Z., Ferdous, S., and Russell, T.P. (2015). Sequential deposition: optimization of solvent swelling for high-performance polymer solar cells. ACS Appl. Mater. Interfaces *7*, 653–661.

171. Aguirre, J.C., Hawks, S.A., Ferreira, A.S., Yee, P., Subramaniyan, S., Jenekhe, S.A., Tolbert, S.H., and Schwartz, B.J. (2015). Sequential processing for organic photovoltaics: design rules for morphology control by tailored semi-orthogonal solvent blends. Adv. Energy Mater. *5*, 1402020.

172. Tang, H., Yan, C., Karuthedath, S., Yin, H., Gao, Y., Gao, J., Zhang, L., Huang, J., So, S.K., Kan, Z., et al. (2020). Deciphering the role of fluorination: morphological manipulation prompts charge separation and reduces carrier recombination in all-small-molecule photovoltaics. Solar RRL *4*, 1900528.

173. Duan, T., Tang, H., Liang, R.-Z., Lv, J., Kan, Z., Singh, R., Kumar, M., Xiao, Z., Lu, S., and Laquai, F. (2019). Terminal group engineering for small-molecule donors boosts the performance of nonfullerene organic solar cells. J. Mater. Chem. A Mater. Energy Sustain. *7*, 2541–2546.

174. Huang, J., Xie, L., Hong, L., Wu, L., Han, Y., Yan, T., Zhang, J., Zhu, L., Wei, Z., and Ge, Z. (2019). Significant influence of halogenation on the energy levels and molecular configurations of polymers in DTBDT-based polymer solar cells. Mater. Chem. Front. *3*, 1244–1252.

175. Jiang, Y., Sun, L., Jiang, F., Xie, C., Hu, L., Dong, X., Qin, F., Liu, T., Hu, L., Jiang, X., et al. (2019). Photocatalytic effect of ZnO on the stability of nonfullerene acceptors and its mitigation by SnO2 for nonfullerene organic solar cells. Mater. Horiz. *6*, 1438–1443.

176. Zhu, X., Hu, L., Wang, W., Jiang, X., Hu, L., and Zhou, Y. (2019). Reversible chemical reactivity of non-fullerene acceptors for organic solar cells under acidic and basic environment. ACS Appl. Energy Mater. *2*, 7602–7608.

177. Xiong, S., Hu, L., Hu, L., Sun, L., Qin, F., Liu, X., Fahlman, M., and Zhou, Y. (2019). 12.5% flexible nonfullerene solar cells by passivating the chemical interaction between the active layer and polymer interfacial layer. Adv. Mater. *31*, e1806616.

178. Park, S., and Son, H.J. (2019). Intrinsic photo-degradation and mechanism of polymer solar cells: the crucial role of non-fullerene acceptors. J. Mater. Chem. A Mater. Energy Sustain. *7*, 25830–25837.

179. Guo, J., Wu, Y., Sun, R., Wang, W., Guo, J., Wu, Q., Tang, X., Sun, C., Luo, Z., Chang, K., et al. (2019). Suppressing photo-oxidation of non-fullerene acceptors and their blends in organic solar cells by exploring material design and employing friendly stabilizers. J. Mater. Chem. A Mater. Energy Sustain. *7*, 25088–25101.

180. Yao, J., Kirchartz, T., Vezie, M.S., Faist, M.A., Gong, W., He, Z., Wu, H., Troughton, J., Watson, T., Bryant, D., et al. (2015). Quantifying losses in open-circuit voltage in solution-processable solar cells. Phys. Rev. Appl. *4*, 014020.

181. Yoshikawa, K., Kawasaki, H., Yoshida, W., Irie, T., Konishi, K., Nakano, K., Uto, T., Adachi, D., Kanematsu, M., Uzu, H., et al. (2017). Silicon heterojunction solar cell with interdigitated back contacts for a photoconversion efficiency over 26%. Nat. Energy *2*, 17032.

182. Liu, Z., Krückemeier, L., Krogmeier, B., Klingebiel, B., Márquez, J.A., Levcenko, S., Öz, S., Mathur, S., Rau, U., Unold, T., et al. (2018). Open-circuit voltages exceeding 1.26 V in planar methylammonium lead iodide perovskite solar cells. ACS Energy Lett. *4*, 110–117.

183. Zhang, Y., Liu, D., Lau, T.K., Zhan, L., Shen, D., Fong, P.W.K., Yan, C., Zhang, S., Lu, X., Lee, C.S., et al. (2020). A novel wide-bandgap polymer with deep ionization potential enables exceeding 16% efficiency in ternary nonfullerene polymer solar cells. Adv. Funct. Mater. *30*, 1910466.

184. Yu, L., Chan, W., Bao, Z., and Cao, S.X.F. (1993). Photorefractive polymers. 2. Structure design and property characterization. Macromolecules *26*, 2216–2221.

185. Bello, K.A., Cheng, L., and Griffiths, J. (1987). Near-infrared absorbing methine dyes based on dicyanovinyl derivatives of indane-i, 3-dione. J. Chem. Soc. 815–818.

186. Yin, H., Chiu, K.L., Bi, P., Li, G., Yan, C., Tang, H., Zhang, C., Xiao, Y., Zhang, H., Yu, W., et al. (2019). Enhanced electron transport and heat transfer boost light stability of ternary organic photovoltaic cells incorporating non-fullerene small molecule and polymer acceptors. Adv. Electron. Mater. *5*, 1900497.

187. Tang, H., Xu, T., Yan, C., Gao, J., Yin, H., Lv, J., Singh, R., Kumar, M., Duan, T., Kan, Z., et al. (2019). Donor derivative incorporation: an effective strategy toward high performance all-small-molecule ternary organic solar cells. Adv. Sci. (Weinh.) *6*, 1901613.

188. Tang, H., Chen, H., Yan, C., Huang, J., Fong, P.W.K., Lv, J., Hu, D., Singh, R., Kumar, M., Xiao, Z., et al. (2020). Delicate morphology control triggers 14.7% efficiency all-small-molecule organic solar cells. Adv. Energy Mater. *10*, 2001076.

189. Li, N., McCulloch, I., and Brabec, C.J. (2018). Analyzing the efficiency, stability and cost potential for fullerene-free organic photovoltaics in one figure of merit. Energy Environ. Sci. *11*, 1355–1361.

190. Machui, F., Hösel, M., Li, N., Spyropoulos, G.D., Ameri, T., Søndergaard, R.R., Jørgensen, M., Scheel, A., Gaiser, D., Kreul, K., et al. (2014). Cost analysis of roll-to-roll fabricated ITO free single and tandem organic solar modules based on data from manufacture. Energy Environ. Sci. *7*, 2792.

191. Guo, J., and Min, J. (2019). A cost analysis of fully solution-processed ITO-free organic solar modules. Adv. Energy Mater. *9*, 1802521.

192. Yue, Q., Liu, W., and Zhu, X. (2020). n-Type molecular photovoltaic materials: design strategies and device applications. J. Am. Chem. Soc. *142*, 11613–11628.